Atmospheric
Chemistry
and Physics

Global inverse modeling of CH₄ sources and sinks: an overview of methods

Sander Houweling[1,2], **Peter Bergamaschi**[3], **Frederic Chevallier**[4], **Martin Heimann**[5], **Thomas Kaminski**[6], **Maarten Krol**[1,2,7], **Anna M. Michalak**[8], **and Prabir Patra**[9]

[1]SRON Netherlands Institute for Space Research, Utrecht, the Netherlands
[2]Institute for Marine and Atmospheric Research (IMAU), Utrecht University, Utrecht, the Netherlands
[3]European Commission Joint Research Centre, Institute for Environment and Sustainability, Ispra (Va), Italy
[4]Le Laboratoire des Sciences du Climat et l'Environnement (LSCE), Gif-Sur-Yvette, France
[5]Max-Planck-Institute for Biogeochemistry, Jena, Germany
[6]The Inversion Lab, Hamburg, Germany
[7]Department of Meteorology and Air Quality (MAQ), Wageningen University and Research Centre, Wageningen, the Netherlands
[8]Department of Global Ecology, Carnegie Institution for Science, Stanford, USA
[9]Japanese Agency for Marine-Earth Science and Technology, Yokohama, Japan

Correspondence to: Sander Houweling (s.houweling@uu.nl)

Abstract. The aim of this paper is to present an overview of inverse modeling methods that have been developed over the years for estimating the global sources and sinks of CH₄. It provides insight into how techniques and estimates have evolved over time and what the remaining shortcomings are. As such, it serves a didactical purpose of introducing apprentices to the field, but it also takes stock of developments so far and reflects on promising new directions. The main focus is on methodological aspects that are particularly relevant for CH₄, such as its atmospheric oxidation, the use of methane isotopologues, and specific challenges in atmospheric transport modeling of CH₄. The use of satellite retrievals receives special attention as it is an active field of methodological development, with special requirements on the sampling of the model and the treatment of data uncertainty. Regional scale flux estimation and attribution is still a grand challenge, which calls for new methods capable of combining information from multiple data streams of different measured parameters. A process model representation of sources and sinks in atmospheric transport inversion schemes allows the integrated use of such data. These new developments are needed not only to improve our understanding of the main processes driving the observed global trend but also to support international efforts to reduce greenhouse gas emissions.

1 Introduction

Thanks to the efforts of surface monitoring networks, the global trends of long-lived greenhouse gases over the past decades are known to high accuracy (Dlugokencky et al., 2009; Prinn et al., 2000; Simpson et al., 2012). However, deciphering the causes of observed growth rate variations remains a challenge, and it is an active field of scientific research and development. The large variations in the methane growth rate that have been observed in the past years are a particularly good example. A wide variety of possible scenarios have been discussed in recent literature, but only limited consensus has been reached so far (Rigby et al., 2008; Bousquet et al., 2011; Monteil et al., 2011; Kai et al., 2011; Aydin et al., 2011; Bergamaschi et al., 2013; Houweling et al., 2014; Turner et al., 2016; Schaefer et al., 2016; Patra et al., 2016; Franco et al., 2016).

The reason why the origin of these growth rate variations is difficult to identify was already discussed extensively dur-

ing the late 1980s and early 1990s, when the first inverse modeling techniques were developed for inferring greenhouse gas sources and sinks from atmospheric measurements (Newsam and Enting, 1988; Enting and Newsam, 1990). The inverse problem was qualified as "ill posed" because of the wide range of surface flux configurations that could explain the measurements about equally as well. Such problems require regularization using a priori assumptions on the surface fluxes needed to fill in critical flux information that the measurement networks are unable to provide.

Since then several approaches have been investigated to strengthen the constraints brought in by the measurements, for example, by increasing the number of data using regional tall tower networks (Bergamaschi et al., 2015; Miller et al., 2013) and satellites (Meirink et al., 2008a; Monteil et al., 2013; Cressot et al., 2014; Wecht et al., 2014) or by using different types of measurements, including methane isotopologues (Mikaloff Fletcher et al., 2004a; Pison et al., 2009; Neef et al., 2010). Accommodating new kinds of data in the inversion framework posed new methodological challenges: not only the computational challenge of solving an inverse problem of significantly increased size was posed but also the treatment of new measurements with poorly quantified error statistics (Houweling et al., 2014). Then, with improved measurement capabilities increasing the flux resolving power of the inversions, transport model uncertainties were recognized to play an increasingly important role (Patra et al., 2011; Kirschke et al., 2013).

Despite methodological limitations, the inverse modeling approach allowed us to derive important constraints on the global sources and sinks of CH$_4$. Examples are the dominant role of the tropical and temperate northern latitudes as drivers of the observed methane increase since 2007 (Bousquet et al., 2011). These constraints exist despite the limited availability of surface measurements in the tropics. The extension of global inversions with satellite retrievals from SCIAMACHY and GOSAT confirmed and even reinforced the importance of tropical fluxes (Frankenberg et al., 2005; Beck et al., 2012; Wilson et al., 2016). Initially, using SCIAMACHY, it took a correction to account for an overestimated role of the tropics due to spectroscopic errors affecting the XCH$_4$ retrieval (Frankenberg et al., 2008). For the boreal and Arctic latitudes, inversions confirm the sensitivity of methane fluxes to climatic variability, but without significant trends in response to global warming yet (Bergamaschi et al., 2013; Bruhwiler et al., 2014). Regarding the atmospheric sink strength, inversions have put bounds on the plausible range of OH interannual variability, although it remains difficult to quantify surface sources and atmospheric sinks independently of each other using the available measurements (Rigby et al., 2008).

The purpose of this paper is to review methods in global inverse modeling of CH$_4$ and directions in which the field is developing. The discussion is limited mostly to global and contemporary methane, although the range of applications has expanded over the years, covering scales ranging from paleoclimate studies (Fischer et al., 2008) to the estimation of single point sources (Kort et al., 2014). Inverse modeling of CH$_4$ has taken advantage of methodological advances gained in the application of inverse modeling to CO$_2$, except for some aspects that are specific to CH$_4$, such as its limited atmospheric lifetime, which will receive special attention.

The next section starts with an overview of how CH$_4$ inversions evolved over the years. The treatment of atmospheric sinks is discussed separately in Sect. 3. Sections 4–6 look closely at the use of isotopic measurements, satellites, and the role of chemistry transport models. Finally, new developments and directions are discussed in Sect. 7.

2   The evolution of methods and estimates

The first inverse modeling analyses of global CH$_4$ made use of concepts and techniques that were developed earlier for studying CO$_2$, as published for example by Enting (1985) and Enting and Mansbridge (1989). The first synthesis of global methane was performed by Fung et al. (1991), who assessed the contribution of various processes to the observed concentrations using a 3-D atmospheric transport model. Sources were not yet optimized using an objective mathematical procedure. Instead, seven scenarios were presented that agreed with the available information on emissions and photochemical oxidation of methane as well as observed quantities, such as global mean CH$_4$, ^{13}CH$_4$, and ^{14}CH$_4$; the amplitudes of their seasonal cycles; and latitudinal gradients.

Brown (1993, 1995) was the first to apply a matrix inversion approach to the available background measurements to derive optimized monthly methane fluxes in 18 latitudinal bands. In Brown (1993) the number of unknowns was kept equal to the number of knowns in order to derive a unique solution. In the follow up study (Brown, 1995) this condition was relaxed through the use of a truncated singular value decomposition approach. Both studies accounted for the atmospheric sink of methane by prescribing model-calculated OH fields, which had been optimized to bring the global lifetime of methyl chloroform (MCF) in agreement with measurements (see for example Spivakovsky et al. (1990)).

Hein et al. (1997) followed the "synthesis inversion" concept of Enting (1993), which made use of a Bayesian formulation of the cost function penalizing deviations from a first guess (a priori) set of CH$_4$ fluxes. In this study, the state vector consisted of global and seasonal patterns of each source and sink process, as well as process-specific δ^{13}C isotopic fractionation factors. Houweling et al. (1999) relaxed the hard constraint on global flux patterns by using the adjoint of the TM2 transport model, coded by Kaminski et al. (1996), to optimize the net CH$_4$ surface flux per month and at the resolution of the transport model. In addition, an attempt was made to take the spatial and temporal correlation of the uncertainty of the monthly fluxes between surrounding grid boxes into account. An iterative procedure was used to mini-

mize the cost function in order to account for the weak non-linearity introduced by optimizing the global OH sink (see Sect. 3). In later studies flux regions have been defined in various ways, ranging between the global patterns of Hein et al. (1997) and the grid-scale fluxes of Houweling et al. (1999), such as the use of 11 continental TransCom regions in Bousquet et al. (2006).

Up to this stage, inverse modeling studies had addressed multiyear mean sources and sinks and their average seasonal variability. For example, the results of Hein et al. (1997) represented a quasi stationary state, reflecting the mean CH$_4$ increase during the analyzed time window of a few years, caused by the mean imbalance between the global sources and sinks during that period. Consistent with this approach, the atmospheric transport model recycled a single representative meteorological year. Important CH$_4$ growth rate fluctuations that were observed in the 1990s, such as in the years after the eruption of Mount Pinatubo and during the strong 1997–1998 El-Niño, raised interest in methods that could address interannual variability. To do this, the use of actual meteorology in atmospheric transport modeling was recognized as being critical, since an important fraction of the observed interannual variability in CH$_4$ could be explained by variability in transport (Warwick et al., 2002).

The first so-called "time-dependent" inversion of methane was published by Mikaloff Fletcher et al. (2004a) using the Kalman filter for the optimization of CH$_4$ fluxes (Bruhwiler et al., 2000). In this inversion, surface emissions were optimized given a scenario for the sinks, i.e., without co-optimizing atmospheric sinks. This approach avoided spurious covariance between the inversion-optimized sources and sinks resulting from the surface network providing insufficient information to constrain these terms independently. Later studies, such as Pison et al. (2009), introduced independent information about the sink through the combined use of CH$_4$ and MCF measurements. Although this approach limits the trade-off between sources and sinks, some degree of influence remains, depending on the weight of the CH$_4$ data relative to those of MCF. The weight of CH$_4$ data increased in particular with the use of satellite data. Several studies using SCIAMACHY satellite retrievals returned to the use of prescribed OH fields (Bergamaschi et al., 2007; Meirink et al., 2008b; Bergamaschi et al., 2009, 2013; Houweling et al., 2014).

The availability of satellite data, starting with the SCIA-MACHY instrument onboard ENVISAT (Bovensmann et al., 1999), triggered new methodological developments to deal with the large number of data becoming available, and it triggered the use of the improved measurement coverage. Several groups adopted the 4D-VAR technique, developed by the weather prediction community, which makes use of the adjoint of the atmospheric transport model for efficient calculation of source receptor relationships and the cost function gradient (Rayner et al., 2016; Chevallier et al., 2005; Baker et al., 2006; Meirink et al., 2008b). With the increasing power of massively parallel super computers, the ensemble Kalman filter (EnKF) gained popularity (Feng et al., 2009; Fraser et al., 2013; Peters et al., 2005; Bruhwiler et al., 2014).

To use satellite data, the inversions were extended with bias correction algorithms to account for systematic errors in the satellite retrievals. Various approaches were tested (see Sect. 5) with spatiotemporally varying bias functions either optimized within the inversion or separately using measurements from the Total Column Carbon Observing Network (TCCON, Wunch et al., 2011a). Because of known short-comings of atmospheric transport models, for example in simulating the stratosphere–troposphere exchange, inversion-optimized bias corrections were found to account in part for model deficiencies (Monteil et al., 2013; Alexe et al., 2015; Locatelli et al., 2015). Compared with CO$_2$, stratosphere–troposphere exchange is relatively important for the column average mixing ratio of CH$_4$ because of the steeper vertical gradient of CH$_4$ in the stratosphere caused by its chemical transformation. Low CH$_4$ mixing ratios in the stratosphere matter because concentration gradients provide the flux information that is used in inversions and should therefore be represented well in models.

The proxy retrieval method, developed for the retrieval of CH$_4$ from SCIAMACHY (Frankenberg et al., 2005), has an additional source of systematic error from the use of transport model output (Parker et al., 2015; Pandey et al., 2016). In this method, XCH$_4$ is derived from the satellite-retrieved ratio of XCH$_4$ and XCO$_2$ to mitigate errors due to light scattering on cirrus and aerosol particles. To translate the retrieved ratios into XCH$_4$, model-derived estimates of XCO$_2$ are used. When proxy retrievals are used in inversions, inaccuracies in the modeled XCO$_2$ variations are projected on the CH$_4$ fluxes (Parker et al., 2015). To deal with this problem, dual CO$_2$ and CH$_4$ inversions were developed, which directly assimilate satellite-retrieved ratios of XCH$_4$ and XCO$_2$ (Fraser et al., 2013; Pandey et al., 2015, 2016), together with surface measurements.

Figure 1 presents large-scale estimates from published global CH$_4$ inversion and how they evolved over time. The global flux is the best-constrained property and shows reasonable consistency across the published studies. The range of estimates reflects mostly the improving capability to constrain the atmospheric oxidation of methane, which was still limited during the 1990s. Brown (1995) explicitly mentions that the difference with Brown (1993) is largely due to the choice of methane lifetime. Notice that the large error margin reported in Brown (1993) is consistent with this difference. Apart from this study, the inversion-derived estimates until 2006 cluster in two groups that differ by 80–100 Tg CH$_4$ yr^{-1}. The global flux estimates in more recent studies suggest that a consensus has been reached in favor of the lower cluster of estimates at 490–520 TgCH$_4$ yr^{-1} for the 1990s. The increasing number of studies covering the period of renewed methane growth show an upward tendency consistent with the CH$_4$ increase. Note that these numbers

are intended to include the soil sink, estimated to be in the range of 26–42 Tg CH$_4$ (Kirschke et al., 2013), but it is not always clear if reported global emissions include or exclude this sink. Furthermore, the use of MCF to constrain tropospheric methane oxidation does not account for the contribution of other potentially important oxidants, such as chlorine radicals in the marine boundary layer (Allan et al., 2005).

The contribution of the Northern Hemisphere to global emissions varies between 67 and 88 % without a clear trend. The differences between the inversions may be explained largely by differences in the interhemispheric exchange rate of the transport models that are used (Patra et al., 2011). In Houweling et al. (1999) the exchange of the TM2 model was found to be too slow, which is consistent with the TM models showing relatively low contributions of northern hemispheric emissions. The anthropogenic contribution varies between 57 and 73 %, with inversions accounting for process-specific information through the use of isotopes showing a smaller range of 60–63 %.

3   Treatment of atmospheric sinks

In this section, we discuss the treatment of atmospheric methane oxidation in inversions. The change in CH$_4$ mixing ratio in an air parcel i due to local sources and sinks is described by

$$\frac{\partial z_i}{\partial t} = E_i - \sum_j k_{i,j}[Ox_j]_i z_i + \sum_l T_l z_l, \tag{1}$$

with z_i and $[Ox_j]_i$ the mixing ratios of CH$_4$ and its main photochemical oxidants OH, Cl, and O(^{1}D), reacting at rate $k_{i,j}$. E_i is the emission into air parcel i and transport operator T_l accounts for the advection and mixing of z_i with its surroundings l (l includes i). The purpose of inverse modeling is to estimate scaling factors $\boldsymbol{x}$ of the surface emissions and chemical transformation rates by fitting mixing ratios simulated by an atmospheric transport model to a set of measurements $\boldsymbol{y}$. The relation between model-simulated measurements $\boldsymbol{z}^f$ and the sources and sinks of CH$_4$ can be expressed as

$$\boldsymbol{z}^f = \mathbf{H}\mathbf{M}_e \boldsymbol{x}_e - \mathbf{H}\mathbf{M}_s \mathbf{Z}\boldsymbol{x}_s + \mathbf{H}\mathbf{M}_0 \mathbf{Z}_0 \boldsymbol{x}_0, \tag{2}$$

where $\mathbf{M}$ is a linear chemistry and transport operator translating the state vector $\boldsymbol{x}$ into model-simulated CH$_4$ mixing ratios $\boldsymbol{z}$, which are sampled using observation operator $\mathbf{H}$ to obtain $\boldsymbol{z}^f$. The notation follows Rayner et al. (2016) as much as possible (see Appendix B), except that we separate the state vector $\boldsymbol{x}$ in its source, sink, and initial concentration components indicated by subscripts "e", "s", and "0". We use $\mathbf{M}$ because the transport model propagates the concentration state, needed to compute the methane sink, from one time step to the next (as in Eq. 1). Matrix $\mathbf{Z}$ is introduced because the state vector components $\boldsymbol{x}_s$ and $\boldsymbol{x}_0$ are usually not defined

at the dimension of the modeled mixing ratios $\boldsymbol{z}$. $\mathbf{Z}$ is defined such that the product $\mathbf{Z}\boldsymbol{x}$ yields $\boldsymbol{z}$ scaled according to the definition of $\boldsymbol{x}$. Note that the model-simulated observations $\boldsymbol{z}^f$ are not linearly dependent on $\boldsymbol{x}_s$ because unlike $\boldsymbol{x}_e$ the sink magnitudes depend on the methane mixing ratios $\boldsymbol{z}$, which are influenced by changes in $\boldsymbol{x}_s$. This introduces a nonlinearity in CH$_4$ inversions that optimizes the transformation rate. In the Bayesian formulation of the cost function, the a priori estimate of $\boldsymbol{x}_s$ is usually derived from a chemistry transport model (CTM). In that model the oxidant abundances also depend on the mixing ratio of CH$_4$, adding further nonlinearity. Following our notation, the CTM changes $[Ox_j]$ in Eq. (1), which is incorporated in $\mathbf{M}_s$ of Eq. (2). This means that when photochemical feedbacks are taken into account, $\mathbf{M}_s$ becomes a nonlinear operator.

Since CH$_4$ is a long-lived gas, i.e., long compared with the typical time window of inversions, the uncertainties in its sources and sinks influence only a small fraction of its average mixing ratio. Therefore, as long as the inversion uses realistic initial concentrations, e.g., derived from the global surface network, and the a priori source and sink estimates are in reasonable balance with the observed global growth rate, the relative changes in $\boldsymbol{z}$ remain minor. In this case, the inverse problem is only weakly nonlinear. As we have seen, the CTM-calculated oxidant fields are usually applied to the inversion after correcting global mean OH to match the measurement-inferred lifetime of MCF of 5.5 ± 0.2 yr (Montzka et al., 2011). This step eliminates any modification of global mean OH in the CTM in response to updated CH$_4$ concentrations coming from the inversion. Because of this, the influence of optimized CH$_4$ mixing ratios on CTM-calculated OH is usually ignored. Aside from global mean OH, it seems reasonable to assume that as long as the relative modifications in CH$_4$ remain small, changes in CTM-calculated OH distributions are not significant.

What remains to be accounted for is the nonlinearity introduced by optimizing the transformation rate $\boldsymbol{x}_s$ within the uncertainty of the methyl chloroform analysis. For this purpose, Eq. (2) can be linearized around an approximation of the CH$_4$ mixing ratios ($\boldsymbol{z}_n$) as follows:

$$\boldsymbol{z}_{n+1}^f = \mathbf{H}\mathbf{M}_e \boldsymbol{x}_{e,n} - \mathbf{H}\mathbf{M}_s \mathbf{Z}_n \boldsymbol{x}_{s,n} + \mathbf{H}\mathbf{Z}_0 \boldsymbol{x}_{0,n}, \tag{3}$$

which can then be used to solve the inverse problem using the iterative procedure

$$\begin{aligned} \boldsymbol{x}_{n+1} = \boldsymbol{x}_n - &\left(\mathbf{M}_n^T \mathbf{H}^T \mathbf{R}^{-1} \mathbf{H}\mathbf{M}_n + \mathbf{B}^{-1} \right)^{-1} \\ &\left(\mathbf{M}_n^T \mathbf{H}^T \mathbf{R}^{-1} \left(\mathbf{H}\mathbf{M}_n \boldsymbol{x}_n - \boldsymbol{y} \right) + \mathbf{B}^{-1} \left(\boldsymbol{x}_n - \boldsymbol{x}^b \right) \right). \end{aligned} \tag{4}$$

Here $\boldsymbol{x}_n$ is a trial state vector after iteration n (combining "e", "s", and "0"). The other elements in this equation follow the standard notation of Rayner et al. (2016). Usually, the a priori CH$_4$ source and sink estimates lead to an atmospheric state that is realistic enough for Eq. (4) to converge within only a few iterations.
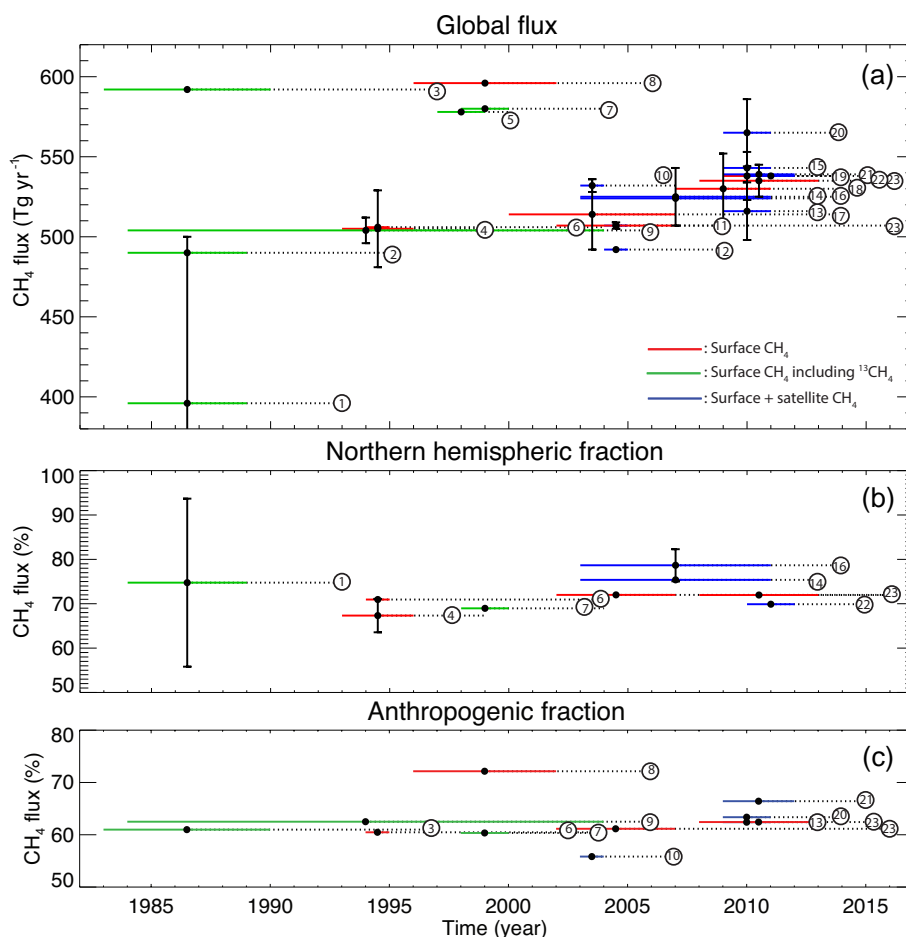
Figure 1. Evolution of inversion-derived estimates for the global total CH$_4$ flux **(a)**, its hemispheric distribution **(b)**, and the anthropogenic contribution **(c)**. Horizontal solid lines indicate the time range of the estimate. The right end of dotted lines point to the date of publication. Note that the CH$_4$ trends that are seen are influenced by the evolution of the inversion methods that were used. Numbered circles refer to publication references, as follows: 1: Brown (1993); 2: Brown (1995); 3: Hein et al. (1997), inv.S0; 4: Houweling et al. (1999); 5: Bergamaschi et al. (2000); 6: Wang et al. (2004); 7: Mikaloff Fletcher et al. (2004b), inv.S2; 8: Chen and Prinn (2006); 9: Bousquet et al. (2006); 10: Bergamaschi et al. (2007), inv.S3; 11: Bergamaschi et al. (2009), inv.S1; 12: Pison et al. (2009); 13: Fraser et al. (2013), inv.3; 14: Bergamaschi et al. (2013), inv.S1SCIA; 15: Monteil et al. (2013), inv.FPNO; 16: Houweling et al. (2014), inv.SQflex; 17: Bruhwiler et al. (2014); 18: Bruhwiler et al. (2014); 19: Cressot et al. (2014), inv.SU$_1^{0.6}$; 20: Cressot et al. (2014), inv.TA$_{0.075}^{0.6}$; 21: Turner et al. (2015); 22: Alexe et al. (2015); 23: Patra et al. (2016).

Equation (4) can be simplified further by ignoring uncertainties in $\boldsymbol{x}_s$ and solving only for surface emissions. In this case the inverse problem becomes linear, and the analytical solution is obtained in a single iteration. If $\boldsymbol{x}_n^g$ is replaced by $\boldsymbol{x}^b$ and $\boldsymbol{x}_{n+1}^g$ by $\boldsymbol{x}^a$ then Eq. (4) indeed reduces to the least squares solution of the linear inverse problem (Tarantola, 2005). The reason why this is commonly done is not primarily out of computational convenience, but rather because surface measurements and satellite-retrieved total columns provide insufficient information to distinguish between source and sink influences. If sources and sinks are optimized simultaneously, solutions are obtained where source adjustments compensate for sink adjustments and vice versa. Depending on the freedom of the inversion to adjust the sink, solutions

will be obtained that show unrealistic compensating adjustments between sources and sinks.

To deal with this problem, MCF measurements are used to independently constrain the sink, either within the inversion (see for example Bousquet et al., 2006) or in a separate inversion preceding the CH$_4$ inversion (see for example Bergamaschi et al., 2009). Usually, this step only optimizes a climatological global OH sink, i.e., ignoring year-to-year variations and uncertainties in its geographical distribution. Given the importance of the methane sinks, their estimated temporal variations (Montzka et al., 2011), and the associated uncertainties (Holmes et al., 2013; Voulgarakis et al., 2013; Naik et al., 2013), these methods are not satisfactory. This will be even more true in the future when MCF mixing ratios

approach a new steady state to unreported residual sources at concentration levels that will be difficult to measure accurately (Lelieveld et al., 2006). We will return to this discussion in Sect. 7.

4 The use of isotopes

Using measurements of CH_4 mixing ratios, only limited information is obtained about source and sink processes. Attempts have been made to use a priori information on spatiotemporal emission patterns to optimize the contribution of specific emission classes. If the state vector is defined at a lower resolution than the model, then the a priori emission distribution within the source regions provides some process-specific information (as in Hein et al., 1997). For inversions that solve at the resolution of the model grid, process-specific flux patterns can be specified only as temporal and spatial correlations in the a priori flux error covariance matrix (as in Bergamaschi et al., 2009), turning this information into a weak constraint. Alternatively, one may just rely on the a priori contribution of each process per grid box and partition the inversion-optimized flux accordingly. However, for CH_4 the a priori patterns themselves are rather uncertain, and therefore it is questionable whether these methods allow any useful process-specific information to be gained from the inversion. The hope may be that this situation will improve in the future with improved measurement coverage, for example, from high-resolution satellite imagers capable of separating source processes geographically.

Alternatively, isotopic measurements provide truly independent process-specific information. For this purpose, several inversion studies used measurements of $\delta^{13}C\text{-}CH_4$ (Brown, 1993, 1995; Hein et al., 1997; Bergamaschi et al., 2000; Mikaloff Fletcher et al., 2004b; Bousquet et al., 2006). So far, however, the impact has been limited because of limitations in network coverage, the low single measurement precision, and differences in calibration standards between laboratories (Levin et al., 2012). Furthermore, this approach requires accurate knowledge of the process-specific isotopic fractionation factors, which are not well separated, for example, for different microbial sources such as ruminants, wetlands, and waste treatment. These factors may also vary strongly for a single-source class depending on specific conditions (Zazzeri et al., 2015; Röckmann et al., 2016). Nevertheless, a rough distinction is possible between the contribution of emissions from microbial sources (wetlands, agriculture, waste processing), energy use (fossil fuel production and consumption), and biomass burning. In addition, measurement techniques are under development with the potential to significantly improve the availability of high-quality data in the future (Röckmann et al., 2016; Eyer et al., 2016).

The additional constraints gained by isotopic measurements can be derived starting from the ^{13}C analogue of Eq. (2):

$$\mathbf{R}_z z^f = \mathbf{HM}_e \mathbf{R}_e x_e - \mathbf{HM}_s \boldsymbol{\alpha}_{12,s}^{13} \mathbf{R}_z \mathbf{Z} x_s + \mathbf{HM}_0 \mathbf{R}_0 \mathbf{Z}_0 x_0, \quad (5)$$

with the diagonal matrix $\mathbf{R}$ containing the $^{13}C / {}^{12}C$ ratios of CH_4. Likewise, $\boldsymbol{\alpha}_{12,s}^{13}$ contains the isotopic fractionation of the oxidation reactions in s. Note that this equation and those that follow also apply to CH_3D. Equation (5) can be reformulated in δ notation as follows:

$$\boldsymbol{\alpha}_z z^f = \mathbf{HM}_e \boldsymbol{\alpha}_e x_e - \mathbf{HM}_s (\boldsymbol{\alpha}_{12,s}^{13} + \boldsymbol{\alpha}_{12,s}^{13} \boldsymbol{\alpha}_z - \mathbf{I}) \mathbf{Z} x_s$$
$$+ \mathbf{HM}_0 \boldsymbol{\alpha}_0 \mathbf{Z}_0 x_0, \quad (6)$$

where $\boldsymbol{\alpha}_z$ and $\boldsymbol{\alpha}_e$ contain the isotopic δ values of atmospheric CH_4 and its emissions, respectively. For the derivation of Eq. (6) see Appendix A. Different approaches are taken for solving inversions using isotopic measurements depending on whether sink strengths and/or δ values are optimized. If both are optimized, the use of isotopic measurements introduces additional nonlinearity since the observed δ values are influenced by the product of source strength and fractionation. In Bousquet et al. (2006), the inverse problem is solved by linearizing Eq. (6) around the first guess state as in Eq. (3) and iteratively solving the problem as in Eq. (4). As in CH_4 inversions where sinks are optimized, the problem is only weakly nonlinear. If the initial state is realistic, subsequent iterations do not modify the solution significantly. As shown in Hein et al. (1997), Eq. (6) can be further simplified with a few approximations taking out the nonlinearity. If sinks and isotopic fractionation constants are not optimized, including the delta value of the initial condition, then the inversion becomes linear again (see, e.g., Mikaloff Fletcher et al., 2004a).

The role of the initial condition in inversions using isotopic measurements has received special attention. Tans (1997) and Lassey et al. (2000) demonstrated that $\delta^{13}C\text{-}CH_4$ takes longer to reach steady state after a perturbation than CH_4 itself. The question was raised how long the spin-up time of inversions should be to avoid errors in the assumed initial concentration field influencing the results. If this time is too short, the inversion may fit the data by compensating errors in the initial condition with artificial emission adjustments. It should be noted, however, that the perturbation recovery time for CH_4 is also much longer than the spin-up time that is used in inversions using only CH_4 data (i.e., without using isotopes). This does not cause problems, as long as the inverse problem is defined such that the initial condition is given sufficient freedom to be optimized itself. The same holds for $^{13}CH_4$ in inversions using isotopic measurements.

Second in importance is the representation of initial spatial gradients that take longest to equilibrate, such as the interhemispheric difference and vertical gradients in the stratosphere. However, as long as these gradient components do not contribute to the global burden (i.e., their global integral adds up to zero), the corresponding relaxation times of both CH_4 and $\delta^{13}C\text{-}CH_4$ remain in the order of the corresponding
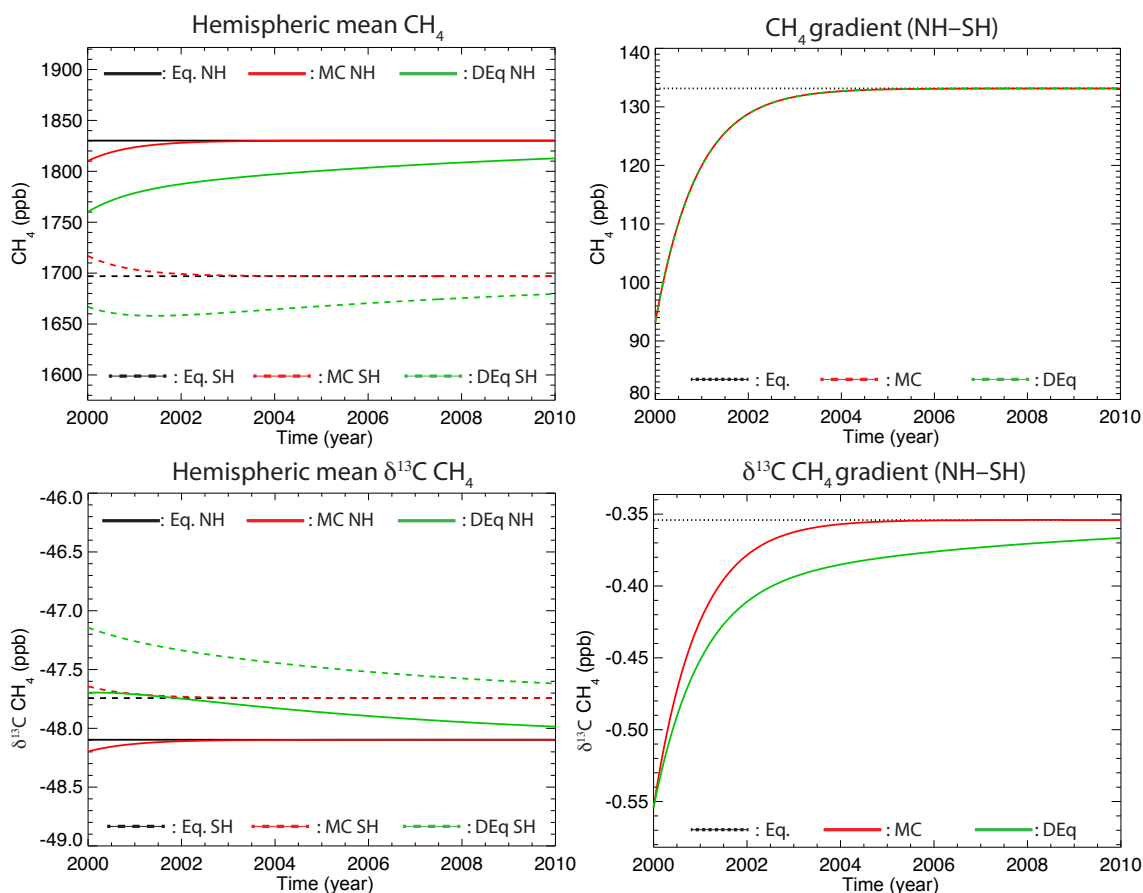
Figure 2. Box-model-calculated relaxation times to hemispheric disturbances in CH$_4$ and ^{13}CH$_4$ with respect to a steady-state equilibrium ("Eq"). Theoretical disturbances of the steady state are either global mass conserved ("MC") or not ("D.Eq").

dynamic mixing times. To demonstrate this point, we performed three simulations using a two-box model with the boxes representing the Northern and Southern hemispheres (see Fig. 2). In the reference simulation the initial condition is in balance with the steady state, and, as expected in this case, nothing changes during the simulation. In a second simulation, the initial concentrations are modified changing the interhemispheric gradient but without changing the global burdens of CH$_4$ and ^{13}CH$_4$. As can be seen, this simulation recovers at the timescale of the interhemispheric exchange (here set to 1 year). Only in the third simulation, where the initial concentrations are perturbed without conserving global mass, the recovery times become of the order of the CH$_4$ lifetime. Interestingly, in this case the north–south gradient of CH$_4$ still recovers at the timescale of interhemispheric mixing, whereas the gradient of δ^{13}C takes much longer to equilibrate.

From this experiment it follows that long relaxation times, and therefore long spin-up times, can be avoided if the inversion is capable of recovering the right initial burdens of CH$_4$ and ^{13}CH$_4$. Therefore, the inversion should be given sufficient freedom to achieve this, i.e to correct errors in the initial global burdens assumed a priori. Additional errors in the global distribution of the initial concentrations call for a spin-up time of the order of the longest dynamical mixing timescale, which is the same for CH$_4$ and δ^{13}C-CH$_4$. The required spin-up time can be reduced further for CH$_4$ and δ^{13}C-CH$_4$ by introducing additional degrees of freedom to the initial condition, such as the difference between the Northern and Southern hemispheres and between the stratosphere and troposphere, such that these gradients can also be optimized from the data.

5 Application to satellite data

The use of satellites in inverse modeling is attractive because of their superior spatial coverage compared with the surface networks. Although a significant step forward has indeed been made using SCIAMACHY and GOSAT, especially in regions that are poorly covered by the surface network, the coverage is still limited by the need for clear sky conditions to retrieve XCH$_4$. In addition, the temporal coverage is limited by the revisit time of the satellite. The most useful remote sensing instruments for the quantification of CH$_4$ emis-

sions from space make use of spectral measurements in the shortwave infrared (SWIR) of Earth-reflected sunlight. Since these photons have traveled the whole atmosphere twice, the measurements are sensitive to CH_4 absorption across the full column down into the planetary boundary layer where the signals of surface emissions are largest (Frankenberg et al., 2005). To obtain sufficient signal puts requirements on the sun angle, which limits the coverage at high latitudes. Techniques exist to further reduce these coverage limitations, e.g., using active instrumentation (Ehret et al., 2008), an elliptical orbit (Nassar et al., 2014), or a large measurement swath (Landgraf et al., 2016), but these have not been tested out in space yet. Therefore, further improvements in measurement coverage are expected for future missions.

To make efficient use of the growing stream of spaceborne greenhouse measurements, inversion methods need adaptation. Important steps in this direction have been taken by the application of the 4D-VAR technique to the inversion of CH_4 emissions (Meirink et al., 2008b; Rayner et al., 2016), which we refer to as the variational approach to avoid confusion about the applicability of "4-D" to the optimization of surface emissions. In this technique, the use of an adjoint model allows evaluation of the cost function gradient at computing time and memory costs that do not scale with the number of measurements, as is the case for the classical matrix inversion technique. However, with the growing information content of the data, a growing number of fluxes can independently be resolved, increasing the required number of iterations. A major limitation of the variational approach is the use of sequential search algorithms to minimize the cost function. Each step in the sequence involves an evaluation of the cost function gradient, requiring a forward and adjoint model simulation for the full time span of the inversion. Because this procedure is strictly sequential, it is difficult to take advantage of the computational power of massive modern parallel computers. Although parallel search algorithms exist (see e.g., Desroziers and Berre, 2012), they have not been applied to CH_4 emission optimization yet. An alternative approach is the use of ensemble methods such as the ensemble Kalman filter (Peters et al., 2007; Bruhwiler et al., 2014), which allows efficient use of large numbers of processors, although the number of regions for which emissions are estimated is still far less compared with the variational approach.

Finding the solution of a large dimensional inverse problem is not the only challenge in using satellite data. Estimating the corresponding posterior uncertainties is an even harder computational problem to solve because methods to approximate the Hessian of the cost function (i.e., the inverse of the posterior covariance matrix; see (Meirink et al., 2008b) for details) tend to converge more slowly than the solution itself. This is true in particular at the smallest spatiotemporal scales that are solved for; hence, the problem is expected to become worse when moving to higher resolutions using instruments that provide more spatiotemporal detail (Meirink et al., 2008b). High-resolution posterior uncer-

tainty estimates are particularly useful in observing system simulation experiments (OSSEs) for testing the performance of inversions using new concepts for measuring greenhouse gases from space (Houweling et al., 2005; Miller et al., 2007; Hungershoefer et al., 2010). A popular method to derive such uncertainties is a Monte Carlo application of the variational approach introduced by Chevallier et al. (2007). This method is computationally demanding, however, because of the large number of inversions needed to determine the posterior uncertainty at a precision of a few % (Pandey et al., 2015). More precise methods exists (Rödenbeck, 2005; Hungershoefer et al., 2010), but they can only be applied to the uncertainty of a limited number of fluxes.

Sampling the model for comparison to satellite retrievals involves application of the retrieval-averaging kernel to the modeled vertical profile of CH_4 as follows:

$$z^f = t_l^T \mathbf{A}_{l,l} z_l + t_l^T (\mathbf{I}_{l,l} - \mathbf{A}_{l,l}) z_l^b. \tag{7}$$

Here the total column operator t_l contains normalized partial columns $\Delta p_i / p_{surf}$ for each layer i of the retrieved profile of l layers. The product of t_l^T and the profile-averaging kernel $\mathbf{A}_{l,l}$ is the column-averaging kernel a_l. If the retrieval uses profile scaling then only a_l is available (see, e.g., Borsdorff et al., 2013). z_l is the modeled vertical profile of methane at the vertical grid of the retrieval. Since the averaging kernel values depend on the vertical discretization of the retrieved state, the model profile should be discretized the same way (i.e., according to the retrieval grid). Furthermore, the averaging kernel depends on the unit in which the state vector (of the retrieval) is expressed, either absorber amount or mixing ratio, and so the model profile has to be expressed accordingly (Deeter et al., 2007). It is advised to correct errors in the CH_4 column amount due to regridding from the vertical grid of the model to that of the retrieval to ensure that the regridding conserves mass. z_l^b is the a priori profile that was used in the retrieval, and $\mathbf{I}_{l,l}$ is the identity matrix. For retrievals that use profile scaling the second right hand side (RHS) term in Eq. (7) should be close to zero (see Borsdorff et al., 2013). Deviations point to the use of a different a priori profile than was used in the retrieval.

For proxy XCH_4 retrievals the use of Eq (7) introduces an additional complication because of the way information about CH_4 and CO_2 is combined. The correct way to deal with this can be readily understood looking at its equation,

$$XCH_4^{proxy} = \frac{XCH_4^{ret}}{XCO_2^{ret}} \times XCO_2^{mod}, \tag{8}$$

showing how the proxy retrieval is derived from the ratio of non-scattering retrievals XCH_4^{ret} and XCO_2^{ret} and a model-derived estimate XCO_2^{mod} as already discussed in Sect. 2. Suppose that XCO_2^{mod} and XCO_2^{ret} were perfect, then the contribution of CO_2 to the RHS of Eq. (8) would cancel out. However, this also requires that the averaging kernel of XCO_2^{ret} is applied to XCO_2^{mod}, which is therefore the correct

way to specify XCO$_2^{\text{mod}}$. What remains is weighted according to the averaging kernel of XCH$_4^{\text{ret}}$, which is the one that should be used when applying Eq. (7) to proxy XCH$_4$ retrievals. In a ratio inversion, Eq. (7) is applied separately to the modeled profiles of CO$_2$ and CH$_4$, after which the ratio of the modeled total columns is taken.

The use of averaging kernels could in theory be avoided by including the radiative transfer model in the inversion, so that the model yields the satellite-observed spectral radiances instead of retrieved mixing ratios. However, for practical reasons this has not been done so far. This approach would avoid inconsistencies between the a priori profile and its uncertainty as used in the retrieval and as generated by the a priori transport model. For further discussion about the statistical consequences of this inconsistency see Chevallier (2015).

A major challenge in the use of satellite data in inversions is to realistically account for uncertainty. Satellite retrievals are influenced by various physical and chemical conditions along the light path that is being measured. Inaccuracies in the capability of the retrieval to take these into account vary at the same spatiotemporal scales as these conditions themselves. They may even correlate with the retrieved variable, like water vapor in the case of SCIAMACHY XCH$_4$ retrievals (Frankenberg et al., 2008; Houweling et al., 2014), which makes it difficult to distinguish signal from error. Errors that behave quasi-random and affect neighboring retrievals in a coherent way can in theory be accounted for by specifying the off-diagonal terms in the data error covariance matrix. In practice, there are many ways to do this, but quantitative information to justify a specific choice is lacking. In general, correlated uncertainty reduces the number of independent measurements, which justifies averaging retrievals within a certain distance of each other. Usually the uncertainty of the mean is calculated using a lower bound representing the contribution of purely systematic error. An alternative approach, referred to as "error inflation", is to increase the error of individually assimilated retrievals such that the uncertainty of a mean of surrounding retrievals does not drop below this minimum level (Chevallier, 2007). The advantage of this approach is that it avoids subjective decisions about which samples to combine into an average. Error inflation, or similar methods that compensate the neglect of off diagonals in the data error covariance matrix by increasing the (diagonal) uncertainty, lead to a χ^2 below 1. Although this may seem suboptimal from a statistical point of view, Chevallier (2007) demonstrated that this de-weighing of data nevertheless leads to uncertainty reductions that are closer to those obtained when off diagonals in **R** had been accounted for. Therefore, this approach avoids over constraining the problem by neglecting the contribution of data error covariance.

As the inversion formalism assumes all errors to be random, measurement bias must be either corrected prior to use in the inversion or be estimated as state vector elements. Both cases require knowledge of the spatiotemporal pattern of the

bias. Given a model representation of the bias **H$'$**, the model-simulated measurements can be reformulated as

$$z^f = \mathbf{HM}x + \mathbf{H}'(x'), \tag{9}$$

where systematic errors are accounted for using a set of extended state vector elements x'. Different formulations of **H$'$**(x') have been used in CH$_4$ inversions using satellite retrievals from GOSAT and SCIAMACHY. Bergamaschi et al. (2007) used simple polynomials of latitude and season to account for inconsistencies arising from the combined use of surface and satellite measurements at large scales. The motivation is that surface measurements are best suited to constrain the large scales, whereas satellite data can be used to fill in regional detail, which the surface network is unable to resolve. An alternative approach (Houweling et al., 2014) is to assess potential causes of systematic error in satellite retrievals, identify the main drivers – or variables that can serve as proxies of their spatiotemporal variation – and optimize the magnitude of the corresponding error contribution in the inversion. It should be noted that the inversion-optimized x'^a has contributions from the measurements as well as systematic errors in the transport model. In addition, if the bias variables co-vary with the XCH$_4$ signal of uncertainties in the surface fluxes, then the inversion will have limited skill in resolving their contributions. To avoid this problem, the TCCON network can be used to optimize the bias model (Wunch et al., 2011b; Houweling et al., 2014). However, because of its sparse global coverage and uncertainties in the TCCON measurements themselves, uncertainties will remain that can be further optimized in the inversion.

6 The importance of transport model uncertainties

An important assumption in inverse modeling is that the influence of atmospheric transport model uncertainties is small compared with the uncertainty of the a priori fluxes. Formally, there are ways to account for transport model uncertainty in the optimization; however, in practice they are difficult to implement when lacking the information required to characterize the statistics of transport model uncertainties in a realistic manner. In addition, there is the fundamental problem that the transport model uncertainty has a significant and poorly quantified systematic component. Patra et al. (2011) assess the importance of transport model uncertainties based on the results of the TransCom-CH$_4$ model intercomparison. The results highlight the importance of specific aspects of atmospheric transport that are critical for the simulation of atmospheric methane, as will be discussed further in this section. Quantifying the impact of transport model differences on inversion-estimated surface fluxes requires an inversion intercomparison. Attempts in this direction have been made, for example by Kirschke et al. (2013). However, in that study inversions were compared without a protocol to standardize the setups. Although useful for an assessment of global

CH$_4$ emissions and uncertainties, isolating the role of transport model uncertainties requires a dedicated experiment. Locatelli et al. (2013) used the output of 10 models participating in the TransCom-CH$_4$ experiment to generate "pseudo measurements" that were inverted in the LMDz model. The results confirm the importance of transport model uncertainties, with estimated annual fluxes on subcontinental scales varying by 23–48 %.

Several studies have highlighted the large contribution of atmospheric transport, including intra and interannual variability, to the observed variability in CH$_4$ (Warwick et al., 2002; Patra et al., 2009; Terao et al., 2011). Because of this, studies that directly relate mixing ratio variations to source variations should be treated with care (see, e.g., Bloom et al., 2010; Turner et al., 2016). For CH$_4$ inversions the observed interhemispheric gradient is of particular importance since it is the dominant mode of variation in background CH$_4$ mixing ratios. The results of Patra et al. (2011) point to a $\sim$50 ppb (40 %) difference in the simulation of this gradient due to differences in model-simulated interhemispheric exchange times. Uncertainty in interhemispheric exchange not only affects the inversion-derived latitudinal distribution of emissions, but also their seasonal cycle in the tropics. The latter is caused by the seasonal dynamics of the intertropical convergence zone (ITCZ). The observed seasonal cycles at tropical measurement sites, such as Samoa and Seychelles, are largely determined by the seasonally varying position of the ITCZ in combination with the size of the north–south gradient of CH$_4$. To assess and improve the interhemispheric exchange in models, SF$_6$ measurements were used (Patra et al., 2011; Monteil et al., 2013). Despite sizable uncertainties in the emission inventory of SF$_6$ (Levin et al., 2010), it nevertheless provides an important constraint on interhemispheric exchange. So far, transport and methane fluxes have been optimized in separate steps, although they could in theory be combined into a single inversion.

Large CH$_4$ gradients are also found in the stratosphere, owing to the long timescale of stratosphere–troposphere exchange in combination with the chemical degradation of CH$_4$ in the stratosphere. The modeling of stratospheric CH$_4$ is gaining importance with the increasing use of satellite data in source–sink inversions. The offline atmospheric transport models that are used for inverse modeling tend to underestimate the residence time (or "age") of stratospheric air (Douglass et al., 2003; Bregman et al., 2006). As a consequence of this, models that accurately reproduce the surface concentrations as observed by the global networks (e.g., after optimization using those data) are expected to overestimate satellite-observed total column CH$_4$ (Locatelli et al., 2015). Since the mean age of stratospheric air varies latitudinally and seasonally, the transport bias varies accordingly. Indeed, the TransCom-CH$_4$ simulations (Patra et al., 2011) show large differences between models, increasing towards higher latitudes in the stratosphere. Although the averaging kernel of SWIR XCH$_4$ retrievals decreases with altitude in the strato-

sphere, transport model differences are large enough to be important for emission quantification. Satellite instruments capable of measuring stratospheric CH$_4$, such as MIPAS and ACE-FTS, are useful for testing models. However, the accuracy of those measurements is also limited (Ostler et al., 2016). A promising development is the use of air core to measure the stratospheric profile of CH$_4$ at high accuracy (Karion et al., 2010), not only to evaluate the accuracy of total column FTS measurements from the TTCON network but also atmospheric transport models. However, because of the observed local variability, which coarse grid models have difficulty reproducing, many balloon flights will be needed to assess and improve, or bias correct, the models.

Using continuous measurements from dense regional networks within Europe and the USA, the large-scale transport problems discussed above are less important. In this case, the observed variability is determined mostly by the passage of fronts of synoptic weather systems and planetary boundary layer (PBL) dynamics. Although the emissions of methane from energy use have some diurnal variation, PBL dynamics are more important especially during summer. Unfortunately, the representation of the nocturnal boundary layer in transport models is too poor to make use of the observed diurnal variability. Instead, measurements are used only during the afternoon when the planetary boundary layer is well developed. Nevertheless, mixing within the PBL and trace gas exchange with the free troposphere is an important source of uncertainty (Kretschmer et al., 2012; Koffi et al., 2016). Since satellite data from sensors operating in the SWIR are only weakly sensitive to the vertical distribution of CH$_4$ in the troposphere, their use may be less sensitive to such errors. The increased coverage and spatial resolution of the new generation of satellite sensors, such as Sentinel 5 precursor TROPOMI (Landgraf et al., 2016), will increase the relevance of satellites for regional-scale emission assessment. These data are highly complementary to surface measurements in the sense that they have a different sensitivity to critical aspects of transport model uncertainty. To bring together regional emission estimates from satellites and surface data is both a major challenge and a great opportunity for testing atmospheric transport.

To assess transport model uncertainties in the simulation of XCH$_4$ we analyzed the archived output of the TransCom-CH$_4$ experiment (Patra et al., 2011) (see Fig. 3). XCH$_4$ fields were calculated from monthly mean mixing ratio output on pressure levels for the year 2000, interpolated to a common horizontal resolution of 2° × 2°. To account for the vertical sensitivity of satellite-retrieved XCH$_4$, we apply averaging kernels from the RemoTeC GOSAT full physics retrieval (Butz et al., 2011). Finally, standard deviations were calculated for each vertical column using results from seven models: ACTM, GEOS-CHEM, MOZART, NIES, PCTM, TM5, and TOMCAT. Figure 3 shows 1-σ differences between the models for the total column, as well as the percentage contribution of stratospheric and tropospheric sub-columns. Re-
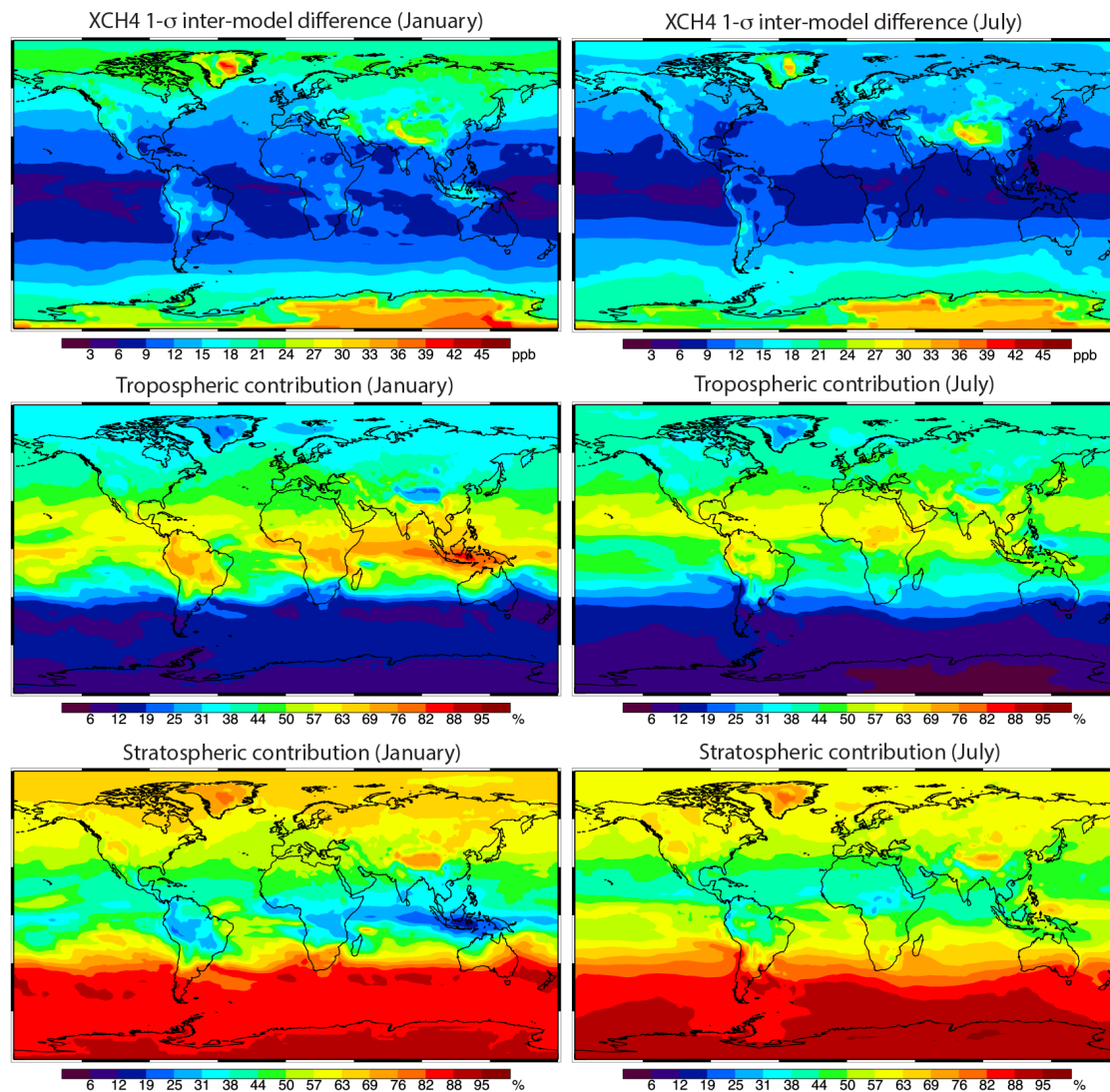
Figure 3. Uncertainty in XCH_4 due to transport model differences for January (left) and July (right). The middle and bottom panels show the percent contribution from the troposphere (1000–200 hPa) and the stratosphere (200–0 hPa) to the total column variability shown in the top panel. Results are obtained using the submissions to the TransCom-CH_4 experiment (Patra et al., 2011) (Control (CTL) tracer for the year 2000).

sults for the total column show σ values up to $\sim 2\%$ (or 35 ppb), associated mostly with steep orography, see, e.g., the Andes, the Himalayas, and most notably the ice caps. The contribution from the troposphere is low in the Southern Hemisphere compared with the Northern Hemisphere because a global offset between the models has been removed at the South Pole. Therefore, the impact of differences in interhemispheric mixing is seen mostly in the Arctic, contributing ~ 10 ppb in XCH_4. The tropospheric contribution to transport model uncertainty also highlights the centers of tropical convection. The contribution of the stratospheric column to the variation in XCH_4 is sizable, and increases towards the poles. The asymmetry between the North and South poles is mainly because of the South Pole correction, taking out

offsets in the SH lower troposphere. It means that the large uncertainties in XCH_4 over Antarctica are caused mainly by the stratosphere. They follow the orography of the ice cap because the impact of the stratospheric sub-column increases as the thickness of the tropospheric sub-column reduces. Towards northern latitudes differences increase up to 50–60 %, highlighting the importance of uncertainty in stratospheric transport when inverting satellite-retrieved total columns.

7 New directions

Compared with the 1990s, when the first inverse modeling studies on CH_4 were published, many things have changed,

most notably the availability of data and computer power. Inverse modeling techniques have been developing further to make use of these advances. Studies used to concentrate on the use of specific data sets, for example, to investigate the use of remote sensing or tall tower networks. Other types of measurements were used to further constrain specific processes, such as the use of MCF to constrain OH or satellite-observed inundation to improve the representation of wetland dynamics. Despite these efforts, the robustness of inverse-modeling-derived estimates is still limited for scales smaller than broad latitudinal bands (Kirschke et al., 2013). Because of this, it remains difficult to attribute the significant changes in the global growth rate that have been observed in the past decades to specific processes. Aside from important efforts to further improve the quality of data and models, there is scope to further explore the combined use of different data sets to further constrain the inverse problem from different directions.

To improve our understanding of what drives the interannual variability in the CH$_4$ growth rate, it is critical to be able to separate influences from varying sources and sinks. To this end, further effort is needed to constrain the atmospheric oxidation of CH$_4$. Since the CH$_4$ and δ^{13}C-CH$_4$ data provide limited constraints on the sink, other data will be needed. The problem with the MCF optimization method is that the two measurement networks, NOAA and AGAGE, lead to different answers, which again differ from chemistry transport model simulations, as demonstrated nicely by Holmes et al. (2013). A better understanding of what causes these differences, including the role of the sparse network for measuring MCF and remaining questions regarding radical recycling in CTMs, is needed (Lelieveld et al., 2016). A promising direction is the use of measurements of other key compounds in photochemistry, such as CO, O$_3$, CH$_2$O, and NO$_x$, to bring the photochemical models into better agreement with the actual observed state (Miyazaki et al., 2012).

Measurements of the vertical profile of CH$_4$ may further improve the separation between surface sources and atmospheric sinks. For this purpose, aircraft measurements are available, as well as satellites that are sensitive to specific altitude ranges, such as IASI (Cressot et al., 2014) and TES (Worden et al., 2012). As discussed in Houweling et al. (1999), applying a uniform scaling of the CH$_4$ lifetime in a transport model influences mostly the interhemispheric gradient and the gradient between stratosphere and troposphere. The transport across these gradients leads to a detectable signal in the upper troposphere, despite the fast vertical mixing within the troposphere. However, because these gradients are small and sensitive to uncertainties in the sub grid parameterization of vertical transport in transport models, it is still a question how effective aircraft profile measurements can be. In the stratosphere the prospects for independent measurement constraints on the sinks are better since the gradients are much larger. It will still require the combined use of CH$_4$ and a chemically inert tracer such as SF$_6$ or CO$_2$ to dis-

tinguish between uncertainties in stratospheric transport and chemistry.

Another approach to separate the influences of sources and sinks is to limit the domain of the inversion to important source regions. In such regions, the concentration signal of the sources varies much more than that of the sink because of the high spatial heterogeneity of CH$_4$ emissions. The sink scales with the total CH$_4$ abundance, which is still dominated by the background. The sources can be quantified, independent of the sink, using short-term departures from the background due to fresh emissions. The influence of the sink on those departures can be neglected because the regional transport times are much shorter than the lifetime of CH$_4$. Meanwhile, several successful attempts have been made to quantify regional CH$_4$ emissions using this approach, for example, using the tall tower networks in Europe (Bergamaschi et al., 2010, 2015) and the USA (Miller et al., 2013; Bruhwiler et al., 2014). Continuous measurements from tall towers record highly variable CH$_4$ concentrations providing much information about regional sources, challenging the performance of high-resolution mesoscale transport models. Despite the challenges, the results demonstrate the potential of this approach for supporting country-scale emission verification.

The use of land surface models to provide a priori emission estimates for use in inverse modeling implies that the concept of carbon cycle data assimilation (CCDAS), which has only been applied to CO$_2$ so far, may also be beneficial for CH$_4$. Aside from the advantage of gaining actual process understanding, which is needed for improved projections of future CH$_4$ concentrations, optimization at process level facilitates the combined use of different types of measurements. In the case of wetland emissions, hydrological conditions are an important driver, particularly in the tropics (Ringeval et al., 2014). Satellite-observed inundation is already used to prescribe the dynamics of the wetland extent (Ringeval et al., 2010; Pison et al., 2013). In combination with hydrological modeling, some limitations of the measurements could be addressed, such as the difficulty to measure water underneath dense vegetation and the fact that wetland soils may be partially saturated but are not necessarily inundated. Improving the representation of wetland emissions in process models will also require extension of the flux measurement network. These measurements would be an essential component of a multi-stream data assimilation system for methane (or MDAS), but the coverage of the network should be more comparable to that of FLUXNET CO$_2$ (Baldocchi et al., 2001). In particular, the model parameterization of methane emissions from tropical wetlands is severely limited by the availability of flux measurements. Such limitations are important to address, but in the meantime the concepts and methods for MDAS should already be developed using the existing data.

Aside from the use of satellites to improve the representation of wetland hydrology, several other kinds of measure-
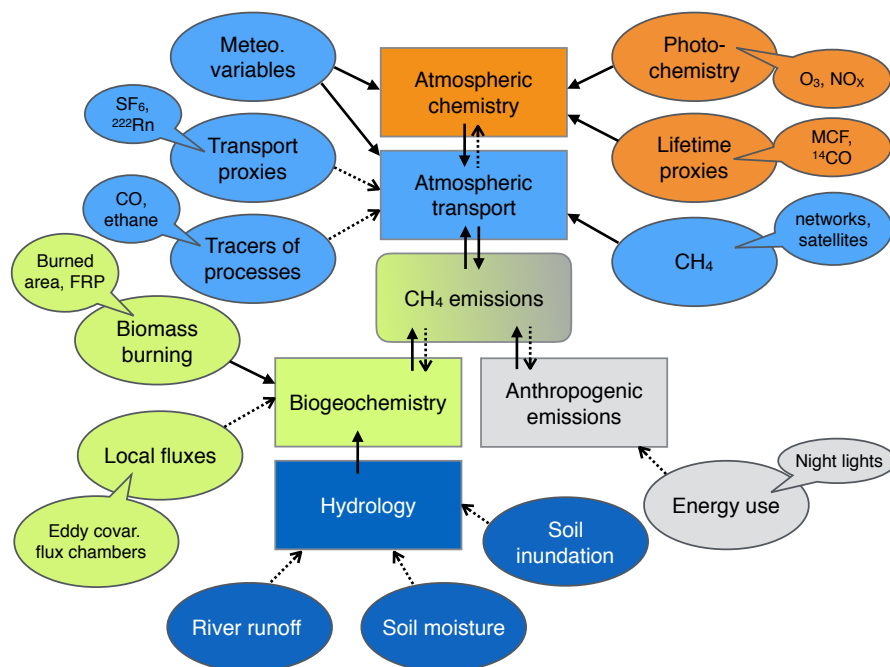
Figure 4. Conceptual diagram of ways to extend the use of measurements in CH₄ flux inversions. Square boxes represent models, ovals represent measurements, and the rounded box represents the target variable of the CH₄ inversion. Call outs provide examples of the kind of measurements that are meant by the ovals (without attempting to be complete). Black arrows: coupled and assimilated into inversions already; dashed arrows: not (yet) coupled or assimilated.

ments can provide process-specific information. For example, atmospheric tracers such as ethane and carbon monoxide provide useful information about emissions from fossil fuel mining (Simpson et al., 2012; Aydin et al., 2011; Hausmann et al., 2016) and biomass burning (Wilson et al., 2016; Bastos et al., 1995), which could be combined with methane measurements in a data assimilation framework. Figure 4 shows a conceptual diagram of how current inversion setups could evolve in order to further increase the constraints on the source and sink processes by using various types of measurements.

8   Closing remarks

In the past 3 decades of CH₄ inverse modeling, important progress has been made in developing atmospheric transport models and inversion methods for the use of various kinds of measurements. Despite this progress, it remains a challenge to identify the dominant drivers of the large global growth rate variations that have been observed during this period. This is caused in part by the difficulty of separating the influence of surface emissions and atmospheric sinks. Breaking up global estimates into regional contributions, the robustness of the estimates decreases further, except in regions where tall tower networks support regional flux estimation. There is no single solution to this problem since every new

approach, such as the use of methane isotopologues or satellite data, brings new information as well as additional unknowns. Making optimal use of the improving observational constraints on atmospheric methane puts increasing demands on the quality of atmospheric transport models. We demonstrated that the use of satellite-retrieved XCH₄ calls for an improved model representation of stratospheric methane.

Aside from the ongoing developments to improve models and measurement data sets, the combined use of different data sets in a single optimization framework is still left largely unexplored. As discussed, the methane budget offers several directions for applying the CCDAS concept to CH₄, on the side of the sources, the sinks, or ideally both. It will be a challenge to combine different data sets in a consistent manner, but inconsistencies will also help identify new directions for improvement. The use of isotopic measurements was discussed as well as how the initial condition can be set up to avoid influences of long isotopic equilibration times.

The COP21 climate agreement offers a great opportunity for inverse modeling to support international efforts to reduce emissions by providing independent estimates to verify if intended reduction targets are being achieved. However, the steps that are needed to become relevant in this process are still sizable. Compared with the achievements of the past 3 decades, it is clear that the overall progress will have to accelerate. To achieve this will require closer international collaboration to make more efficient use of the collective ef-

fort that is spent by different research groups already. The annual assessments of GCP-CH$_4$ (Saunois et al., 2016) are an important first step in this direction.

Appendix A: Isotopic equation in delta notation

To derive Eq. (6) from Eq. (5) we first subtract Eq. (2), multiplied with a reference isotopic ration $\mathbf{R}_{\text{ref}}$, from Eq. (5) resulting in

$$
\begin{aligned}
(\mathbf{R}_z - \mathbf{R}_{\text{ref}})\, z^f = {} & \mathbf{HM}_e\, (\mathbf{R}_e - \mathbf{R}_{\text{ref}})\, \boldsymbol{x}_e \\
& - \mathbf{HM}_s\left(\boldsymbol{\alpha}^{13}_{12,s}\mathbf{R}_z - \mathbf{R}_{\text{ref}}\right)\mathbf{Z}\boldsymbol{x}_s \\
& + \mathbf{HM}_0\,(\mathbf{R}_0 - \mathbf{R}_{\text{ref}})\,\mathbf{Z}_0\boldsymbol{x}_0.
\end{aligned}
\tag{A1}
$$

To transfer to delta notation we substitute $\mathbf{R}$ in Eq. (A1) using

$$
\mathbf{R}_x = (\mathbf{I} + \boldsymbol{\alpha}_x)\mathbf{R}_{\text{VPDB}},
\tag{A2}
$$

where subscript x refers to any specific occurrence of $\mathbf{R}$ in Eq. (A1) and $\mathbf{R}_{\text{VPDB}}$ is the isotopic ratio of the Vienna Pee Dee Belemnite international reference standard. Note that since we are using matrix notation $\mathbf{R}$ represents a diagonal matrix of isotopic ratios (the same applies to $\boldsymbol{\alpha}$). After substitution and dividing by $\mathbf{R}_{\text{VPDB}}$, we obtain

$$
\begin{aligned}
(\boldsymbol{\alpha}_z - \boldsymbol{\alpha}_{\text{ref}})z^f = {} & \mathbf{HM}_0(\boldsymbol{\alpha}_e - \boldsymbol{\alpha}_{\text{ref}})\boldsymbol{x}_e \\
& - \mathbf{HM}_s\left(\boldsymbol{\alpha}^{13}_{12,s}\boldsymbol{\alpha}_z + \boldsymbol{\alpha}^{13}_{12,s} - (\boldsymbol{\alpha}_{\text{ref}} + \mathbf{I})\right)\mathbf{Z}\boldsymbol{x}_s \\
& + \mathbf{HM}_0(\boldsymbol{\alpha}_0 - \boldsymbol{\alpha}_{\text{ref}})\mathbf{Z}_0\boldsymbol{x}_0.
\end{aligned}
\tag{A3}
$$

Depending on the choice of $\boldsymbol{\alpha}_{\text{ref}}$, different formulations can be derived. Equation (6) is derived using $\boldsymbol{\alpha}_{\text{ref}} = 0$.

Appendix B: Notation

Table of notation, taken from Rayner et al. (2016, Table 1, page 4).

Basic notation symbol	Description
BOLD	Matrix
bold	Vector
x	Target variables for assimilation
z	Model state variables
y	Vector of observations
J	Cost function
$\mathbf{U}(x, x^t)$	Uncertainty covariance of x around some reference point x^t
$\mathbf{C}(x)$	Uncertainty correlation of x
$p(x)$	Probability density function evaluated at x
$G(x, \mu, \mathbf{U})$	Multivariate normal (Gaussian) distribution with mean μ and covariance $\mathbf{U}$
H	Observation operator mapping model state onto observables
$\mathbf{H}$	Jacobian of H, often used in its place, especially for linear problems
M	Model to evolve state vector from one timestep to the next
$\mathbf{M}$	Jacobian of M
$(\cdot)^a$	Posterior or analysis
$(\cdot)^b$	Background or prior
$(\cdot)^f$	Forecast
$(\cdot)^g$	(First) guess in iteration
$(\cdot)^t$	True
δ	Increment

Useful shortcut symbols	Description
d	$y - \mathbf{H}(x)$ (Innovation)
$\mathbf{U}(x)$	Uncertainty covariance of x about its own mean, i.e., the true uncertainty covariance
$\mathbf{B}$	$\mathbf{U}(x^b)$ (Prior uncertainty covariance)
$\mathbf{Q}$	$\mathbf{U}(x^f, x^t)$ (Forecast uncertainty covariance)
$\mathbf{R}$	$\mathbf{U}(y - \mathbf{H}(x^t))$ (Innovation uncertainty covariance)
$\mathbf{A}$	$\mathbf{U}(x^a)$ (Posterior uncertainty covariance)

References

Alexe, M., Bergamaschi, P., Segers, A., Detmers, R., Butz, A., Hasekamp, O., Guerlet, S., Parker, R., Boesch, H., Frankenberg, C., Scheepmaker, R. A., Dlugokencky, E., Sweeney, C., Wofsy, S. C., and Kort, E. A.: Inverse modelling of CH$_4$ emissions for 2010–2011 using different satellite retrieval products from GOSAT and SCIAMACHY, Atmos. Chem. Phys., 15, 113–133, doi:10.5194/acp–15–113–2015, 2015.

Allan, W., Lowe, D. C., Gomez, A. J., Struthers, H., and Brailsford, G. W.: Interannual variation of ^{13}C in tropospheric methane: Implications for a possible atomic chlorine sink in the marine boundary layer, J. Geophys. Res., 110, doi:10.1029/2004JD005650, 2005.

Aydin, M., Verhulst, K. R., Saltzman, E. S., Battle, M. O., Montzka, S. A., Blake, D. R., Tang, Q., and Prather, M. J.: Recent decreases in fossil-fuel emissions of ethane and methane derived from firn air, Nature, 476, 198–201, doi:10.1038/nature10352, 2011.

Baker, D. F., Doney, S. D., and Schimel, D. S.: Variational data assimilation for atmospheric CO$_2$, Tellus B, 58, 359–365, 2006.

Baldocchi, D., Falge, E., Gu, L. H., Olson, R., Hollinger, D. et al.: FLUXNET: A new tool to study the temporal and spatial variability of ecosystem-scale carbon dioxide, water vapor, and energy flux densities, Bull. Am. Met. Soc., 82, 2415–2434, doi:10.1175/1520-0477, 2001.

Bastos, A., Running, S. W., Gouveia, C., and Trigo, R. M.: The global NPP dependence on ENSO: La Niña and the extraordinary year of 2011, J. Geophys. Res., 118, 1247–1255, doi:10.1002/jgrg.20100, 1995.

Beck, V., Chen, H., Gerbig, C., Bergamaschi, P., Bruhwiler, L., Houweling, S., Röckmann, T., Kolle, O., Steinbach, J., Koch, T., Sapart, C. J., van der Veen, C., Frankenberg, C., Andreae, M. O., Artaxo, P., Longo, K. M., and Wofsy, S. C.: Methane airborne measurements and comparison to global models during BARCA, J. Geophys. Res., 117, D15310, doi:10.1029/2011JD017345, 2012.

Bergamaschi, P., Bräunlich, M., Marik, T., and Brenninkmeijer, C. A. M.: Measurements of the carbon and hydrogen isotopes of atmospheric methane at Izāna, Tenerife: Seasonal cycles and synoptic-scale variations, J. Geophys. Res., 105, 14531–14546, 2000.

Bergamaschi, P., Frankenberg, C., Meirink, J. F., Krol, M., Dentener, F., Wagner, T., Platt, U., Kaplan, J. O., Körner, S., Heimann, M., Dlugokencky, E. J., and Goede, A.: Satellite chartography of atmospheric methane from SCIAMACHY on board ENVISAT: 2. Evaluation based on inverse model simulations, J. Geophys. Res., 112, doi:10.1029/2006JD007268, 2007.

Bergamaschi, P., Frankenberg, C., Meirink, J.-F., Krol, M., Gabriella Villani, M., Houweling, S., Dentener, F., Dlugokencky, E. J., Miller, J. B., Gatti, L. V., Engel, A., and Levin, I.: Inverse modeling of global and regional CH$_4$ emissions using SCIAMACHY satellite retrievals, J. Geophys. Res., 114, D22301, doi:10.1029/2009JD012287, 2009.

Bergamaschi, P., Krol, M., Meirink, J. F., Dentener, F., Segers, A., van Aardenne, J., Monni, S., Vermeulen, A. T., Schmidt, M., Ramonet, M., Yver, C., Meinhardt, F., Nisbet, E. G., Fisher, R. E., O'Doherty, S., and Dlugokencky, E. J.: Inverse modeling of European CH$_4$ emissions 2001–2006, J. Geophys. Res., 115, D22309, doi:10.1029/2010JD014180, 2010.

Bergamaschi, P., Houweling, S., Segers, A., Krol, M., Frankenberg, C., Scheepmaker, R. A., Dlugokencky, E., Wofsy, S. C., Kort, E. A., Sweeney, C., Schuck, T., Brenninkmeijer, C., Chen, H., Beck, V., and Gerbig, C.: Atmospheric CH$_4$ in the first decade of the 21st century: Inverse modeling analysis using SCIAMACHY satellite retrievals and NOAA surface measurements, J. Geophys. Res., 118, 7350–7369, doi:10.1002/jgrd.50480, 2013.

Bergamaschi, P., Corazza, M., Karstens, U., Athanassiadou, M., Thompson, R. L., Pison, I., Manning, A. J., Bousquet, P., Segers, A., Vermeulen, A. T., Janssens-Maenhout, G., Schmidt, M., Ramonet, M., Meinhardt, F., Aalto, T., Haszpra, L., Moncrieff, J., Popa, M. E., Lowry, D., Steinbacher, M., Jordan, A., O'Doherty, S., Piacentino, S., and Dlugokencky, E.: Top-down estimates of European CH$_4$ and N$_2$O emissions based on four different inverse models, Atmos. Chem. Phys., 15, 715–736, doi:10.5194/acp-15-715-2015, 2015.

Bloom, A., Palmer, P. I., Fraser, A., Reay, D. S., and Frankenberg, C.: Large-scale controls methanogenesis inferred from methane and gravity spaceborne data, Science, 327, 322–325, 2010.

Borsdorff, T., Hasekamp, O. P., Wassmann, A., and Landgraf, J.: Remote sensing of atmospheric trace gas columns: An efficient approach for regularization and calculation of total column averaging kernels, Atmos. Meas. Tech., 7, 523–535, doi:10.5194/amt-7-523-2014, 2014.

Bousquet, P., Ciais, P., Miller, J. B., Dlugokencky, E. J., Hauglustaine, D. A., Prigent, C., Van der Werf, G. R., Peylin, P., Brunke, E.-G., Carouge, C., Langenfelds, R. L., Lathière, J., Papa, F., Ramonet, M., Schmidt, M., Steele, L. P., Tyler, S. C., and White, J.: Contribution of anthropogenic and natural sources to atmospheric methane variability, Nature, 443, 439–443, doi:10.1038/nature05132, 2006.

Bousquet, P., Ringeval, B., Pison, I., Dlugokencky, E. J., Brunke, E.-G., Carouge, C., Chevallier, F., Fortems-Cheiney, A., Frankenberg, C., Hauglustaine, D. A., Krummel, P. B., Langenfelds, R. L., Ramonet, M., Schmidt, M., Steele, L. P., Szopa, S., Yver, C., Viovy, N., and Ciais, P.: Source attribution of the changes in atmospheric methane for 2006–2008, Atmos. Chem. Phys., 11, 3689–3700, doi:10.5194/acp-11-3689-2011, 2011.

Bovensmann, H., Burrows, J. P., Buchwitz, M., Frerick, J., Noël, S., Rozanov, V. V., Chance, K. V., and Goede, A. P. H.: SCIAMACHY: Mission objectives and measurement modes, J. Atmos. Sci., 56, 127–150, 1999.

Bregman, B., Meijer, E., and Scheele, R.: Key aspects of stratospheric tracer modeling using assimilated winds, Atmos. Chem. Phys., 6, 4529–4543, doi:10.5194/acp-6-4529-2006, 2006.

Brown, M.: Deduction of emissions of source gases using an objective inversion algorithm and a chemical transport model, J. Geophys. Res., 98, 12639–12660, 1993.

Brown, M.: The singular value decomposition method applied to the deduction of the emissions and the isotopic composition of atmospheric methane, J. Geophys. Res., 100, 11425–11446, 1995.

Bruhwiler, L., Tans, P., and Ramonet, M.: A time-dependent assimilation and source retrieval technique for atmospheric tracers, in: Inverse Methods in Global Biogeochemical Cycles, edited by: Kasibhatla, P. , AGU, Washington, DC, Geophys. Monogr. Ser., 114, 265–277, 2000.

Bruhwiler, L., Dlugokencky, E., Masarie, K., Ishizawa, M., Andrews, A., Miller, J., Sweeney, C., Tans, P., and Worthy, D.: CarbonTracker-CH$_4$: an assimilation system for estimating emissions of atmospheric methane, Atmos. Chem. Phys., 14, 8269–8293, doi:10.5194/acp–14–8269–2014, 2014.

Butz, A., Guerlet, S., Hasekamp, O., Schepers, D., Galli, A., Aben, I., Frankenberg, C., Hartmann, J. M., Tran, H., Kuze, A., Keppel-Aleks, G., Toon, G., Wunch, D., Wennberg, P., Deutscher, N., Griffith, D., Macatangay, R., Messerschmidt, J., Notholt, J., and Warneke, T.: Toward accurate CO$_2$ and CH$_4$ observations from GOSAT, Geophys. Res. Lett., 38, L14812, doi:10.1029/2011GL047888, 2011.

Chen, Y. and Prinn, R. G.: Estimation of atmospheric methane emissions between 1996 and 2001 using a three-dimensional global chemical transport model, J. Geophys. Res., 111, JD006058, doi:10.1029/2005JD006058, 2006.

Chevallier, F.: Impact of correlated observation errors on inverted CO$_2$ surface fluxes from OCO measurements, Geophys. Res. Lett., 34, L24804, doi:10.1029/2007GL030463, 2007.

Chevallier, F.: On the statistical optimality of CO$_2$ atmospheric inversions assimilating CO$_2$ column retrievals, Atmos. Chem. Phys., 15, 11133–11145, doi:10.5194/acp-15-11133-2015, 2015.

Chevallier, F., Fisher, M., Peylin, P., Serrar, S., Bousquet, P., Breon, F. M., Chedin, A., and Ciais, P.: Inferring CO$_2$ sources and sinks from satellite observations: Method and application to TOVS data, J. Geophys. Res., 110, D24309, doi:10.1029/2005JD006390, 2005.

Chevallier, F., Bréon, F.-M., and Rayner, P. J.: Contribution of the Orbiting Carbon Observatory to the estimation of CO$_2$ sources and sinks: Theoretical study in a variational data assimilation framework, J. Geophys. Res., 112, D09307, doi:10.1029/2006JD007375, 2007.

Cressot, C., Chevallier, F., Bousquet, P., Crevoisier, C., Dlugokencky, E. J., Fortems-Cheiney, A., Frankenberg, C., Parker, R., Pison, I., Scheepmaker, R. A., Montzka, S. A., Krummel, P. B., Steele, L. P., and Langenfelds, R. L.: On the consistency between global and regional methane emissions inferred from SCIAMACHY, TANSO-FTS, IASI and surface measurements, Atmos. Chem. Phys., 14, 577–592, doi:10.5194/acp–14–577–2014, 2014.

Deeter, M. N., Edwards, D. P., Gille, J. C., and Drummond, J. R.: Sensitivity of MOPITT observations to carbon monoxide in the lower troposphere, J. Geophys. Res., 112, doi:10.1029/2007JD008929, 2007.

Desroziers, G. and Berre, L.: Accelerating and parallelizing minimizations in ensemble and deterministic variational assimilations, Q. J. R. Meteorol. Soc., 138, 1599–1610, doi:10.1002/qj.1886, 2012.

Dlugokencky, E. J., Bruhwiler, L., White, J. W. C., Emmons, L. K., Novelli, P. C., Montzka, S. A., Masarie, K. A., Lang, P. M., Crotwell, A. M., Miller, J. B., and Gatti, L. V.: Observational constraints on recent increases in the atmospheric CH$_4$ burden, Geophys. Res. Lett., 36, L18803, doi:10.1029/2009GL039780, 2009.

Douglass, A. R., Schoeberl, M. R., and Rood, R. B.: Evaluation of transport in the lower tropical stratosphere in a global chemistry and transport model, J. Geophys. Res., 108, 4259, doi:10.1029/2002JD002696, 2003.

Ehret, G., Kiemle, C., Wirth, M., Amediek, A., Fix, A., and Houweling, S.: Space-borne remote sensing of CO$_2$, CH$_4$, and N$_2$O by integrated path differential absorption lidar: a sensitivity analysis, Appl. Phys. B, 90, 593–608, doi:10.1007/s00340-007-2892-3, 2008.

Enting, I. G.: A classification of some inverse problems in geochemical modeling, Tellus B, 37, 216–229, 1985.

Enting, I. G.: Inverse problems in atmospheric constituent studies, III. Estimating errors in surface sources, Inverse problems, 9, 649–665, 1993.

Enting, I. G. and Mansbridge, J. V.: Seasonal sources and sinks of atmospheric CO$_2$; direct inversion of filtered data, Tellus B, 41, 111–126, 1989.

Enting, I. G. and Newsam, G. N.: Atmospheric constituent inversion problems: Implications for baseline monitoring, J. Atmos. Chem., 11, 69–87, 1990.

Eyer, S., Tuzson, B., Popa, M. E., van der Veen, C., Röckmann, T., Rothe, M., Brand, W. A., Fisher, R., Lowry, D., Nisbet, E. G., Brennwald, M. S., Harris, E., Zellweger, C., Emmenegger, L., Fischer, H., and Mohn, J.: Real-time analysis of δ^{13}C and δD-CH$_4$ in ambient air with laser spectroscopy: method development and first intercomparison results, Atmos. Meas. Tech., 9, 263–280, doi:10.5194/amt-9-263-2016, 2016.

Feng, L., Palmer, P. I., Bösch, H., and Dance, S.: Estimating surface CO$_2$ fluxes from space-borne CO$_2$ dry air mole fraction observations using an ensemble Kalman Filter, Atmos. Chem. Phys., 9, 2619–2633, doi:10.5194/acp-9-2619-2009, 2009.

Fischer, H., Behrens, M., Bock, M., Richter, U., Schmitt, J., Loulergue, L., Chappellaz, J., Spahni, R., Blunier, T., Leuenberger, M., and Stocker, T. F.: Changing boreal methane sources and constant biomass burning during the last termination, Nature, 452, 864–867, doi:10.1038/nature06825, 2008.

Franco, B., Mahieu, E., Emmons, L. K., Tzompa-Sosa, Z. A., Fischer, E. V., Sudo, K., Bovy, B., Conway, S., Griffin, D., Hannigan, J. W., Strong, K., and Walker, K. A.: Evaluating ethane and methane emissions associated with the development of oil and natural gas extraction in North America, Environ. Res. Lett., 11, doi:10.1088/1748-9326/11/4/044010, 2016.

Frankenberg, C., Meirink, J. F., van Weele, M., Platt, U., and Wagner, T.: Assessing Methane Emissions from Global Space-Borne Observations, Science, 3008, 1010–1014, 2005.

Frankenberg, C., Bergamaschi, P., Butz, A., Houweling, S., Meirink, J.-F., Notholt, J., Petersen, A. K., Schrijver, H., Warneke, T., and Aben, I.: Tropical methane emissions: A revised view from SCIAMACHY onboard ENVISAT, Geophys. Res. Lett., 35, L15811, doi:10.1029/2008GL034300, 2008.

Fraser, A., Palmer, P. I., Feng, L., Boesch, H., Cogan, A., Parker, R., Dlugokencky, E. J., Fraser, P. J., Krummel, P. B., Langenfelds, R. L., O'Doherty, S., Prinn, R. G., Steele, L. P., van der Schoot, M., and Weiss, R. F.: Estimating regional methane surface fluxes: the relative importance of surface and GOSAT mole

fraction measurements, Atmos. Chem. Phys., 13, 5697–5713, doi:10.5194/acp-13-5697-2013, 2013.

Fung, I., John, J., Lerner, J., Matthews, E., Prather, M., Steele, L. P., and Fraser, P. J.: Three-dimensional model synthesis of the global methane cycle, J. Geophys. Res., 96, 13033–13065, 1991.

Hausmann, P., Sussmann, R., and Smale, D.: Contribution of oil and natural gas production to renewed increase in atmospheric methane (2007–2014): top–down estimate from ethane and methane column observations, Atmos. Chem. Phys., 16, 3227–3244, doi:10.5194/acp-16-3227-2016, 2016.

Hein, R., Crutzen, P. J., and Heimann, M.: An inverse modeling approach to investigate the global atmospheric methane cycle, Global Biogeochem. Cy., 11, 43–76, 1997.

Holmes, C. D., Prather, M. J., Sövde, O. A., and Myhre, G.: Future methane, hydroxyl, and their uncertainties: key climate and emission parameters for future predictions, Atmos. Chem. Phys., 13, 285–302, doi:10.5194/acp-13-285-2013, 2013.

Houweling, S., Kaminski, T., Dentener, F. J., Lelieveld, J., and Heimann, M.: Inverse modeling of methane sources and sinks using the adjoint of a global transport model, J. Geophys. Res., 104, 26137–26160, 1999.

Houweling, S., Hartmann, W., Aben, I., Schrijver, H., Skidmore, J., and Roelofs, G.-J.: Evidence of systematic errors in SCIAMACHY-observed CO$_2$ due to aerosols, Atmos. Chem. Phys., 5, 3003–3013, doi:10.5194/acp-5-3003-2005, 2005.

Houweling, S., Krol, M., Bergamaschi, P., Frankenberg, C., Dlugokencky, E. J., Morino, I., Notholt, J., Sherlock, V., Wunch, D., Beck, V., Gerbig, C., Chen, H., Kort, E. A., Röckmann, T., and Aben, I.: A multi-year methane inversion using SCIAMACHY, accounting for systematic errors using TCCON measurements, Atmos. Chem. Phys., 14, 3991–4012, doi:10.5194/acp–14–3991–2014, 2014.

Hungershoefer, K., Breon, F.-M., Peylin, P., Chevallier, F., Rayner, P., Klonecki, A., Houweling, S., and Marshall, J.: Evaluation of various observing systems for the global monitoring of CO$_2$ surface fluxes, Atmos. Chem. Phys., 10, 10503–10520, doi:10.5194/acp-10-10503-2010, 2010.

Kai, F. M., Tyler, S. C., Randerson, J. T., and Blake, D. R.: Reduced methane growth rate explained by decreased Northern Hemisphere microbial sources, Nature, 476, 194–197, doi:10.1038/nature10259, 2011.

Kaminski, T., Heimann, M., and Giering, R.: Sensitivity of the seasonal cycle of CO$_2$ at remote monitoring stations with respect to seasonal surface exchange fluxes determined with the adjoint of an atmospheric transport model, Phys. Chem. Earth, 21, 457–462, 1996.

Karion, A., Sweeney, C., Tans, P., and Newberger, T.: AirCore: An Innovative Atmospheric Sampling System, J. Atmos. Oceanic Technol., 27, 1839–1853, doi:10.1175/2010JTECHA1448.1, 2010.

Kirschke, S., Bousquet, P., Ciais, P., Saunois, M., Canadell, J. G. et al.: Three decades of global methane sources and sinks, Nat. Geosci., 6, 813–823, doi:10.1038/ngeo1955, 2013.

Koffi, E. N., Bergamaschi, P., Karstens, U., Krol, M., Segers, A., Schmidt, M., Levin, I., Vermeulen, A. T., Fisher, R. E., Kazan, V., Klein Baltink, H., Lowry, D., Manca, G., Meijer, H. A. J., Moncrieff, J., Pal, S., Ramonet, M., Scheeren, H. A., and Williams, A. G.: Evaluation of the boundary layer dynamics of the TM5 model over Europe, Geosci. Model Dev., 9, 3137–3160, doi:10.5194/gmd-9-3137-2016, 2016.

Kort, E. A., Frankenberg, C., Costigan, K. R., Lindenmaier, R., Dubey, M. K., and Wunch, D.: Four corners: The largest US methane anomaly viewed from space, Geophys. Res. Lett., 41, 6898–6903, doi:10.1002/2014GL061503, 2014.

Kretschmer, R., Koch, F.-T., Feist, D. G., Biavati, G., Karstens, U., and Gerbig, C.: Toward Assimilation of Observation-Derived Mixing Heights to Improve Atmospheric Tracer Transport Models, in: Lagrangian Modeling of the Atmosphere, edited by: Lin, J., Brunner, D., Gerbig, C., Stohl, A., Luhar, A., and Webley, P., American Geophysical Union, Washington DC, doi:10.1029/2012GM001255, 2012.

Landgraf, J., aan de Brugh, J., Scheepmaker, R., Borsdorff, T., Hu, H., Houweling, S., Butz, A., Aben, I., and Hasekamp, O.: Carbon monoxide total column retrievals from TROPOMI shortwave infrared measurements, Atmos. Meas. Tech., 9, 4955–4975, doi:10.5194/amt-9-4955-2016, 2016.

Lassey, K. R., Lowe, D. C., and Manning, M. R.: The trend in atmospheric methane δ^{13}C and implications for isotopic constraints on the global methane budget, Global Biogeochem. Cy., 14, 41–49, doi:10.1029/1999GB900094, 2000.

Lelieveld, J., Brenninkmeijer, C. A. M., Jöckel, P., Isaksen, I. S. A., Krol, M. C., Mak, J. E., Dlugokencky, E., Montzka, S. A., Novelli, P. C., Peters, W., and Tans, P. P.: New Directions: Watching over tropospheric hydroxyl (OH), Atmos. Environ., 40, 5741–5743, 2006.

Lelieveld, J., Gromov, S., Pozzer, A., and Taraborrelli, D.: Global tropospheric hydroxyl distribution, budget and reactivity, Atmos. Chem. Phys., 16, 12477–12493, doi:10.5194/acp-16-12477-2016, 2016.

Levin, I., Naegler, T., Heinz, R., Osusko, D., Cuevas, E., Engel, A., Ilmberger, J., Langenfelds, R. L., Neininger, B., v. Rohden, C., Steele, L. P., Weller, R., Worthy, D. E., and Zimov, S. A.: The global SF$_6$ source inferred from long-term high precision atmospheric measurements and its comparison with emission inventories, Atmos. Chem. Phys., 10, 2655–2662, doi:10.5194/acp-10-2655-2010, 2010.

Levin, I., Veidt, C., Vaughn, B. H., Brailsford, G., Bromley, T., Heinz, R., Lowe, D., Miller, J. B., Poss, C., and White, J. W. C.: No inter-hemispheric d^{13}CH$_4$ trend observed, Nature, 486, E3–E4, doi:10.1038/nature11175, 2012.

Locatelli, R., Bousquet, P., Chevallier, F., Fortems-Cheney, A., Szopa, S., Saunois, M., Agusti-Panareda, A., Bergmann, D., Bian, H., Cameron-Smith, P., Chipperfield, M. P., Gloor, E., Houweling, S., Kawa, S. R., Krol, M., Patra, P. K., Prinn, R. G., Rigby, M., Saito, R., and Wilson, C.: Impact of transport model errors on the global and regional methane emissions estimated by inverse modelling, Atmos. Chem. Phys., 13, 9917–9937, doi:10.5194/acp-13-9917-2013, 2013.

Locatelli, R., Bousquet, P., Saunois, M., Chevallier, F., and Cressot, C.: Sensitivity of the recent methane budget to LMDz subgrid-scale physical parameterizations, Atmos. Chem. Phys., 15, 9765–9780, doi:10.5194/acp-15-9765-2015, 2015.

Meirink, J.-F., Bergamaschi, P., Frankenberg, C., d'Amelio, M. T. S., Dlugokencky, E. J., Gatti, L. V., Houweling, S., Miller, J. B., Röckmann, T., Villani, M. G., and Krol, M. C.: Four-dimensional variational data assimilation for inverse modeling of atmospheric methane emissions: Analysis of

SCIAMACHY observations, J. Geophys. Res., 113, D17301, doi:10.1029/2007JD009740, 2008a.

Meirink, J. F., Bergamaschi, P., and Krol, M. C.: Four-dimensional variational data assimilation for inverse modelling of atmospheric methane emissions: Method and comparison with synthesis inversion, Atmos. Chem. Phys., 8, 6341–6353, doi:10.5194/acp-8-6341-2008, 2008b.

Mikaloff Fletcher, S. E., Tans, P. P., Bruhwiler, L. M., Miller, J. B., and Heimann, M.: CH_4 sources estimated from atmospheric observations of CH_4 and its $^{13}C / ^{12}C$ isotopic ratios: 1. Inverse modeling of source processes, Global Biogeochem. Cy., 18, 1–17, doi:10.1029/2004GB002223, 2004a.

Mikaloff Fletcher, S. E., Tans, P. P., Bruhwiler, L. M., Miller, J. B., and Heimann, M.: CH_4 sources estimated from atmospheric observations of CH_4 and its $^{13}C / ^{12}C$ isotopic ratios: 2. Inverse modeling of CH_4 fluxes from geographical regions, Global Biogeochem. Cy., 18, 1–15, doi:10.1029/2004GB002224, 2004b.

Miller, J. B., Gatti, L. V., d'Amelio, M. T. S., Crotwell, A. M., Dlugokencky, E. J., Bakwin, P., Artaxo, P., and Tans, P. P.: Airborne measurements indicate large methane emissions from the eastern Amazon basin, Geophys. Res. Lett., 34, 1–5, doi:10.1029/2006GL029213, 2007.

Miller, S. M., Wofsy, S. C., Michalak, A. M., Kort, E. A., Andrews, A. E., Biraud, S. C., Dlugokencky, E. J., Eluszkiewicz, J., Fischer, M. L., Janssens-Maenhout, G., Miller, B. R., Miller, J. B., Montzka, S. A., Nehrkorn, T., and Sweeney, C.: Anthropogenic emissions of methane in the United States, PNAS, 110, 20018–20022, 2013.

Miyazaki, K., Eskes, H. J., Sudo, K., Takigawa, M., van Weele, M., and Boersma, K. F.: Simultaneous assimilation of satellite NO_2, O_3, CO, and HNO_3 data for the analysis of tropospheric chemical composition and emissions, Atmos. Chem. Phys., 12, 9545–9579, doi:10.5194/acp-12-9545-2012, 2012.

Monteil, G., Houweling, S., Dlugockenky, E. J., Maenhout, G., Vaughn, B. H., White, J. W. C., and Röckmann, T.: Interpreting methane variations in the past two decades using measurements of CH_4 mixing ratio and isotopic composition, Atmos. Chem. Phys., 11, 9141–9153, doi:10.5194/acp-11-9141-2011, 2011.

Monteil, G., Houweling, S., Guerlet, S., Schepers, D., Frankenberg, C., Scheepmaker, R., Aben, I., Butz, A., Hasekamp, O., Landgraf, J., Wofsy, S. C., and Röckmann, T.: Intercomparison of 15 months inversions of GOSAT and SCIAMACHY CH_4 retrievals, J. Geophys. Res., 118, 11807–11823, doi:10.1002/2013JD019760, 2013.

Montzka, S. A., Krol, M., Dlugokencky, E. J., Hall, B., Joeckel, P., and Lelieveld, J.: Small Interannual Variability of Global Atmospheric Hydroxyl, Science, 331, 67–69, 2011.

Naik, V., Voulgarakis, A., Fiore, A. M., Horowitz, L. W., Lamarque, J.-F. et al.: Preindustrial to present-day changes in tropospheric hydroxyl radical and methane lifetime from the Atmospheric Chemistry and Climate Model Intercomparison Project (ACCMIP), Atmos. Chem. Phys., 13, 5277–5298, doi:10.5194/acp-13-5277-2013, 2013.

Nassar, R., Sioris, C. E., Jones, D. B. A., and McConnell, J. C.: Satellite observations of CO_2 from a highly elliptical orbit for studies of the Arctic and boreal carbon cycle, J. Geophys. Res., 119, 2654–2673, doi:10.1002/2013JD020337, 2014.

Neef, L., van Weele, M., and van Velthoven, P.: Optimal estimation of the present-day global methane budget, Global Biogeochem. Cy., 24, doi:10.1029/2009GB003661, 2010.

Newsam, G. N. and Enting, I. G.: Inverse problems in atmospheric constituent studies, I., Determination of surface sources under a diffusive transport approximation, Inverse Prob., 4, 1037–1054, 1988.

Ostler, A., Sussmann, R., Patra, P. K., Houweling, S., De Bruine, M., Stiller, G. P., Haenel, F. J., Plieninger, J., Bousquet, P., Yin, Y., Saunois, M., Walker, K. A., Deutscher, N. M., Griffith, D. W. T., Blumenstock, T., Hase, F., Warneke, T., Wang, Z., Kivi, R., and Robinson, J.: Evaluation of column-averaged methane in models and TCCON with a focus on the stratosphere, Atmos. Meas. Tech., 9, 4843–4859, doi:10.5194/amt-9-4843-2016, 2016.

Pandey, S., Houweling, S., Krol, M., Aben, I., and Röckmann, T.: On the use of satellite-derived $CH_4 : CO_2$ columns in a joint inversion of CH_4 and CO_2 fluxes, Atmos. Chem. Phys., 15, 8615–8629, doi:10.5194/acp-15-8615-2015, 2015.

Pandey, S., Houweling, S., Krol, M., Aben, I., Chevallier, F., Dlugokencky, E. J., Gatti, L. V., Gloor, E., Miller, J. B., Detmers, R., Machida, T., and Röckmann, T.: Inverse modeling of GOSAT-retrieved ratios of total column CH_4 and CO_2 for 2009 and 2010, Atmos. Chem. Phys., 16, 5043–5062, doi:10.5194/acp-16-5043-2016, 2016.

Parker, R. J., Boesch, H., Byckling, K., Webb, A. J., Palmer, P. I., Feng, L., Bergamaschi, P., Chevallier, F., Notholt, J., Deutscher, N., Warneke, T., Hase, F., Sussmann, R., Kawakami, S., Kivi, R., T., D. W., Griffith, and Velazco, V.: Assessing 5 years of GOSAT Proxy XCH4 data and associated uncertainties, Atmos. Meas. Tech., 8, 4785–4801, doi:10.5194/amt-8-4785-2015, 2015.

Patra, P. K., M, T., Ishijima, K., Choi, B. C., a.D Cunnold, Dlugokencky, E. J., Fraser, P., Gomez-Pelaez, A. J., Goo, T. Y., Kim, J. S., Krummel, P., Langenfelds, R., Mukai, H., O'Doherty, S., Prinn, R. G., Simmonds, P., Steele, P., Tohjima, Y., Tsuboi, K., Uhse, K., Weiss, R., Worthy, D., and Nakazawa, T.: Growth Rate, Seasonal, Synoptic, Diurnal Variations and Budget of Methane in the Lower Atmosphere, J. Met. Soc. Japan, 87, 635–663, doi:10.2151/jmsj.87.635, 2009.

Patra, P. K., Houweling, S., Krol, M., Bousquet, P., Belikov, D., Bergmann, D., Bian, H., Cameron-Smith, P., Chipperfield, M. P., Corbin, K., Fortems-Cheiney, A., Fraser, A., Gloor, E., Hess, P., Ito, A., Kawa, S. R., Law, R. M., Loh, Z., Maksyutov, S., Meng, L., Palmer, P. I., Prinn, R. G., Rigby, M., Saito, R., and Wilson, C.: TransCom model simulations of CH_4 and related species: linking transport, surface flux and chemical loss with CH_4 variability in the troposphere and lower stratosphere, Atmos. Chem. Phys., 11, 12813–12837, doi:10.5194/acp-11-12813-2011, 2011.

Patra, P. K., Saeki, T., Dlugokencky, E. J., Ishijima, K., Umezawa, T., Ito, A., Aoki, S., Morimoto, S., Kort, E. A., Crotwell, A., Ravi Kumar, K., and Nakazawa, T.: Regional Methane Emission Estimation Based on Observed Atmospheric Concentrations (2002–2012), J. Met. Soc. Jap., 94, 91–112, doi:10.2151/jmsj.2016-006, 2016.

Peters, W., Miller, J. B., Whitaker, J., Denning, A. S., Hirsch, A., Krol, M. C., Zupanski, D., Bruhwiler, L., and Tans, P. P.: An ensemble data assimilation system to estimate CO_2 surface fluxes from atmospheric trace gas observations, J. Geophys. Res., 110, doi:10.1029/2005JD006157, 2005.

Peters, W., Jacobson, A. R., Sweeney, C., Andrews, A. E., Conway, T. J., Masarie, K., Miller, J. B., Bruhwiler, L. M. P., Petron, G., Hirsch, A. I., Worthy, D. E. J., van der Werf, G. R., Randerson, J. T., Wennberg, P. O., Krol, M. C., and Tans, P. P.: An atmospheric perspective on North American carbon dioxide exchange: CarbonTracker, Proc. Natl. Acad. Sci., 104, 18925–18930, 2007.

Pison, I., Bousquet, P., Chevallier, F., Szopa, S., and Hauglustaine, D.: Multi-species inversion of CH$_4$, CO and H$_2$ emissions from surface measurements, Atmos. Chem. Phys., 9, 5281–5297, doi:10.5194/acp-9-5281-2009, 2009.

Pison, I., Ringeval, B., Bousquet, P., Prigent, C., and Papa, F.: Stable atmospheric methane in the 2000s: key-role of emissions from natural wetlands, Atmos. Chem. Phys., 13, 11609–11623, doi:10.5194/acp-13-11609-2013, 2013.

Prinn, R. G., Weiss, R. F., Fraser, P. J., Simmonds, P. G., Cunnold, D. M., Alyea, F. N., O'Doherty, S., Salameh, P., Miller, B. R., Huang, J., Wang, R. H. J., Hartley, D. E., Harth, C., Steele, L. P., Sturrock, G., Midgley, P. M., and McCulloch, A.: A history of chemically and radiatively important gases in air deduced from ALE/GAGE/AGAGE, J. Geophys. Res., 105, 17751–17792, 2000.

Rayner, P., Michalak, A. M., and Chevallier, F.: Fundamentals of Data Assimilation, Geosci. Model Dev. Discuss., doi:10.5194/gmd-2016-148, in review, 2016.

Rigby, M., Prinn, R. G., Fraser, P. J., Simmonds, P. G., Langenfelds, R. L., Huang, J., Cunnold, D. M., Steele, L. P., Krummel, P. B., Weiss, R. F., O'Doherty, S., Salameh, P. K., Wang, H. J., Harth, C. M., Mühle, J., and Porter, L. W.: Renewed growth of atmospheric methane, Geophys. Res. Lett., 35, doi:10.1029/2008GL036037, 2008.

Ringeval, B., de Noblet-Ducoudré, N., Ciais, P., Bousquet, P., Prigent, C., Papa, F., and Rossow, W. B.: An attempt to quantify the impact of changes in wetland extent on methane emissions on the seasonal and interannual time scales, Global Biogeochem. Cy., 24, doi:10.1029/2008GB003354, 2010.

Ringeval, B., Houweling, S., van Bodegom, P. M., Spahni, R., van Beek, R., Joos, F., and Röckmann, T.: Methane emissions from floodplains in the Amazon basin: Challenges in developing a process-based model for global applications, Biogeosciences, 11, 1519–1558, doi:10.5194/bg-11-1519-2014, 2014.

Röckmann, T., Eyer, S., van der Veen, C., Popa, M. E., Tuzson, B., Monteil, G., Houweling, S., Harris, E., Brunner, D., Fischer, H., Zazzeri, G., Lowry, D., Nisbet, E. G., Brand, W. A., Necki, J. M., Emmenegger, L., and Mohn, J.: In situ observations of the isotopic composition of methane at the Cabauw tall tower site, Atmos. Chem. Phys., 16, 10469–10487, doi:10.5194/acp-16-10469-2016, 2016.

Rödenbeck, C.: Estimating CO$_2$ sources and sinks from atmospheric mixing ratio measurements using a global inversion of atmospheric transport, Tech. Rep. 6 ISSN 1615-7400, Max-Planck-Institut für Biogeochemie, Jena, Germany, 2005.

Saunois, M., Bousquet, P., Poulter, B., Peregon, A., Ciais, P. et al.: The global methane budget 2000–2012, Earth Syst. Sci. Data, 8, 697–751, doi:10.5194/essd-8-697-2016, 2016.

Schaefer, H., Mikaloff Fletcher, S. E., Veidt, C., Lassey, K. R., Brailsford, G. W., Bromley, T. M., Dlugokencky, E. J., Michel, S. E., Miller, J. B., Levin, I., Lowe, D. C., Martin, R. J., Vaughn, B. H., and White, J. W. C.: A 21st-century shift from fossil-fuel to biogenic methane emissions indicated by ^{13}CH$_4$, Science, 352, 80–84, 2016.

Simpson, O. J., Sulbaek, M. P., Meinardi, A. S., Bruhwiler, L., Blake, N. J., Helmig, D., Sherwood Rowland, F., and Blake, D. R.: Long-term decline of global atmospheric ethane concentrations and implications for methane, Nature, 491, doi:10.1038/nature11342, 2012.

Spivakovsky, C. M., Yevich, J. A., Logan, A., Wofsy, S. C., McElroy, M. B., and Prather, M. J.: Tropospheric OH in a three dimensional chemical tracer model: an assessment based on observations of CH$_3$CCl$_3$, J. Geophys. Res., 95, 18411–18471, 1990.

Tans, P. P.: A note on isotopic ratios and the global atmospheric methane budget, Global Biogeochem. Cy., 11, 77–81, 1997.

Tarantola, A.: Inverse problem theory, and methods for model parameter estimation, Society for Industrial and Applied Mathematics, Philadelphia, 2005.

Terao, Y., Mukai, H., Nojiri, Y., Machida, T., Tohjima, Y., Saeki, T., and Maksyutov, S.: Interannual variability and trends in atmospheric methane over the western Pacific from 1994 to 2010, J. Geophys. Res., 116, D14303, doi:10.1029/2010JD015467, 2011.

Turner, A. J., Jacob, D. J., Wecht, K. J., Maasakkers, J. D., Lundgren, E., Andrews, A. E., Biraud, S. C., Boesch, H., Bowman, K. W., Deutscher, N. M., Dubey, M. K., Griffith, D. W. T., Hase, F., Kuze, A., Notholt, J., Ohyama, H., Parker, R., Payne, V. H., Sussmann, R., Sweeney, C., Velazco, V. A., Warneke, T., Wennberg, P. O., and Wunch, D.: Estimating global and North American methane emissions with high spatial resolution using GOSAT satellite data, Atmos. Chem. Phys., 15, 7049–7069, doi:10.5194/acp-15-7049-2015, 2015.

Turner, A. J., Jacob, D. J., Benmergui, J., Wofsy, S. C., Maasakkers, J. D., Butz, A., Hasekamp, O., Biraud, S. C., and Dlugokencky, E.: A large increase in US methane emissions over the past decade inferred from satellite data and surface observations, Geophys. Res. Lett., 43, 2218–2224, doi:10.1002/2016GL067987, 2016.

Voulgarakis, A., Naik, V., Lamarque, J.-F., Shindell, D. T., Young, P. J., Prather, M. J., Wild, O., Field, R. D., Bergmann, D., Cameron-Smith, P., Cionni, I., Collins, W. J., Dalsøren, S. B., Doherty, R. M., Eyring, V., Faluvegi, G., Folberth, G. A., Horowitz, L. W., Josse, B., MacKenzie, I. A., Nagashima, T., Plummer, D. A., Righi, M., Rumbold, S. T., Stevenson, D. S., Strode, S. A., Sudo, K., Szopa, S., and Zeng, G.: Analysis of present day and future OH and methane lifetime in the ACCMIP simulations, Atmos. Chem. Phys., 13, 2563–2587, doi:10.5194/acp-13-2563-2013, 2013.

Wang, J. S., Logan, J. A., McElroy, M. B., Duncan, B. N., Megretskaia, I. A., and Yantosca, R. M.: A 3-D model analysis of the slowdown and interannual variability in the methane growth rate from 1988 to 1997, Global Biogeochem. Cy., 18, GB3011, doi:10.1029/2003GB002180, 2004.

Warwick, N. J., Bekki, S., Law, K. S., Nisbet, E. G., and Pyle, J. A.: The impact of meteorology on the interannual growth rate of atmospheric methane, Geophys. Res. Lett., 29, doi:10.1029/2002GL015282, 2002.

Wecht, K. J., Jacob, D. J., Frankenberg, C., Jiang, Z., and Blake, D. R.: Mapping of North American methane emissions with high spatial resolution by inversion of SCIAMACHY satellite data, J. Geophys. Res., 119, 7741–7756, doi:10.1002/2014JD021551, 2014.

Wilson, C., Gloor, M., Gatti, L. V., Miller, J. B., Monks, S. A., Mc-Norton, J., Bloom, A. A., Basso, L. S., and Chipperfield, M. P.: Contribution of regional sources to atmospheric methane over the Amazon Basin in 2010 and 2011, Global Biogeochem. Cy., 30, 400–420, doi:10.1002/2015GB005300, 2016.

Worden, J., Kulawik, S., Frankenberg, C., Payne, V., Bowman, K., Cady-Peirara, K., Wecht, K., Lee, J.-E., and Noone, D.: Profiles of CH$_4$, HDO, H$_2$O, and N$_2$O with improved lower tropospheric vertical resolution from Aura TES radiances, Atmos. Meas. Tech., 5, 397–411, doi:10.5194/amt-5-397-2012, 2012.

Wunch, D., Toon, G. C., Blavier, J.-F. L., Washenfelder, R. A., Notholt, J., Connor, B. J., Griffith, D. W. T., Sherlock, V., and Wennberg, P. O.: The total carbon column observing network, Phil. Trans. R. Soc., 369, 2087–2112, doi:10.1098/rsta.2010.0240, 2011a.

Wunch, D., Wennberg, P. O., Toon, G. C. et al.: A method for evaluating bias in global measurements of CO$_2$ total columns from space, Atmos. Chem. Phys., 11, 12317–12337, 2011b.

Zazzeri, G., Lowry, D., Fisher, R. E., France, J. L., Lanoisellé, M., and Nisbet, E. G.: Plume mapping and isotopic characterisation of anthropogenic methane sources, Atmos. Environ., 110, 151–162, doi:10.1016/j.atmosenv.2015.03.029, 2015.